SIGNAL ANALYSIS USING THE WARPED DISCRETE FOURIER TRANSFORM

By

OHBONG KWON

A DISSERTATION PRESENTED TO THE GRADUATE SCHOOL
OF THE UNIVERSITY OF FLORIDA IN PARTIAL FULFILLMENT
OF THE REQUIREMENTS FOR THE DEGREE OF
DOCTOR OF PHILOSOPHY

UNIVERSITY OF FLORIDA

2010

To my Family

ACKNOWLEDGMENTS

This dissertation is the result of many years of work whereby I have been accompanied and supported by many people. Therefore, their appreciation is well-deserved. First and foremost, I would like to sincerely thank my advisor Dr. Fred J. Taylor for his excellent support, encouragement and consideration in guiding the research.

I would also like to thank all the members of my advisory committee: Dr. Herman Lam, Dr. Janise McNair and Dr. Douglas Cenzer for their valuable time and interest in serving on my supervisory committee as well as their advice and comments, which helped improve the quality of this dissertation.

Lastly, I could not thank enough to my parents who gently offered unconditional support, and encouragements at each turn of the road. Their love has enabled me to complete this process as well as grow from it.

TABLE OF CONTENTS

LIST OF TABLES

LIST OF FIGURES

ABSTRACT OF DISSERTATION PRESENTED TO THE GRADUATE SCHOOL OF THE UNIVERSITY OF FLORIDA IN PARTIAL FULFILLMENT OF THE REQUIREMENTS FOR THE DEGREE OF DOCTOR OF PHILOSOPHY

SPECTRAL ANALSYS USING THE WARPED DISCRETE FOURIER TRANSFORM

By

Ohbong Kwon

May 2010

Chair: Fred J. Taylor
Major: Electrical and Computer Engineering

In this dissertation, we present a multi-tone signal processing paradigm that is based on the use of the warped discrete Fourier transform (WDFT). The WDFT evaluates a discrete-time signal in the context of a non-uniform frequency spectrum, a process called warping. Compared to a conventional DFT or FFT, which produces a spectrum having uniform frequency resolution across the entire baseband, the WDFT's frequency resolution is both non-uniform and programmable. This feature is exploited for use in analyzing multi-tone signals which are problematic to the DFT/FFT. This dissertation focuses on optimizing frequency discrimination by determining the best warping strategy and control by using the intelligent search algorithms and criteria of optimization, or cost functional. The system developed and tested focuses on maximizing the SDFT frequency resolution over those frequencies that exhibit a localized concentration of spectral energy and, implicitly, diminishing the importance of other frequency ranges. This dissertation demonstrates that by externally controlling the frequency resolution of the WDFT in an intelligent manner, multi-tone signals can be more readily detected and classified. Furthermore, the WDFT can be built upon an FFT enabled framework, insuring high efficiency and bandwidths.

CHAPTER 1
INTRODUCTION

1.1 Background

Multi-tone signal detection and discrimination is a continuing signal processing problem. The applications include dual-tone multi-frequency (DTMF) systems, Doppler radar, electronic countermeasures, wireless communications, and OFDM-based radar exciters, to name but a few. Traditional multi-tone detection systems are often based on a filter bank architecture that uses an array of product modulators to heterodyne signals down to DC, and then processes the array of down-converters that serve as a bank of lowpass filters [1]. The outputs of the filter bank are then processed using a suite of energy detection operations to detect the presence of multiple input tones [2]. The capability of such a system to isolate and detect multiple narrowband signals is predicated on the choice of initial modulating frequencies and post-processing algorithms. Other approaches to the signal discrimination problem are based on multiple signal classification (MUSIC) algorithms, least mean-square (LMS) estimators, and windowed and unwindowed DFTs and their derivatives, such as Goertzel algorithm [3]. The DFT or DFT variant decomposes a signal into a fixed set of frequency harmonics that are uniformly spaced over the normalized baseband. A variation of the DFT theme has been suggested to provide a more flexible choice of the frequencies. In the modulated DFT system, for example, the input sequence is modulated before the signal is presented to a conventional DFT [4]. As a result, all frequency samples are shifted by a fixed amount, giving uniformly spaced frequencies starting with any arbitrary value. Another instance is the notch Fourier transform which assumes that the input consists of a few sinusoids of arbitrary frequencies and then employs a few notch filters that are

used to compute the corresponding Fourier coefficients [5]. The target harmonics are, however, limited in number. For applications demanding exponential frequency samples, digital frequency warping, which provides unequal spectral bandwidth has also been suggested [6].

The approach taken in this dissertation is to explore the use of a specific DFT derivative called the warped discrete Fourier transform or WDFT [7]. The WDFT will be shown to decompose a signal into a frequency domain signature having a non-uniform frequency spectrum.

1.2 Research Contributions

The major objectives of the research are to explore the use of the WDFT as multi-tone signal detection technology, assess its capabilities, and compare its performance to other established techniques. It should be appreciated that a salient difference between a DFT and WDFT is frequency resolution. The traditional DFT possesses a uniform frequency resolution across the entire baseband. That means that the resolution of the DFT depends on the spacing between two consecutive frequency harmonics and that an increase in the frequency resolution can be obtained by increasing the DFT length. However, an increase in the DFT length will also increase the computational complexity and thereby reduce the real-time capabilities of the system. On the other hand, the frequency resolution of the WDFT is non-uniform and externally controlled (programmable). This feature will be used to overcome the multi-tone signal detection limitation of the uniform resolution DFT. By intelligently and locally controlling the frequency resolution of the WDFT it is anticipated that a high level of signal discrimination can be achieved. What needs to be accomplished is to develop an

adaptive “steering” algorithm that will place the highest WDFT resolution in the frequency range containing the signals of interest.

The first contribution of this dissertation is to reduce spectral leakage due to the finite frequency resolution of the DFT without increasing the DFT length for multi-tone detection using the WDFT. As a matter of fact, an increase in the DFT length improves the sampling accuracy by reducing the spectral separation of adjacent DFT samples, while it causes higher computational complexity and cost penalty. The WDFT can control the spectral separation through the warping parameter so as to minimize spectral leakage

The second contribution is to obtain higher and optimized local frequency resolution using the WDFT through finding the best warping control strategy. In general, a uniformly windowed DFT/FFT cannot determine if one tone or multiple tones are present locally about a harmonic frequency for two tones separated by 1.6 Δ (1.6 harmonics) or less. It will be shown that the WDFT can discriminate between two signals separated by as little as 1.3 harmonics.

1.3 Organization of the Dissertation

The dissertation is organized as follows: In Chapter 2, we provide a general overview of spectral analysis and its limitations. Chapter 3 introduces the Discrete Fourier Transform and the Warped Discrete Fourier Transform. Chapter 4 presents the simple WDFT example using the first-order allpass filter and shows some cases according to the warping parameter using the MATLAB. In Chapter 5, we briefly summarize the traditional uniform DFT filter banks and introduce the non-uniform DFT filter banks using an allpass filter transformation. Chapter 6 reports the outcome of preliminary studies regarding WDFT-based multi-tone signal detection and optimization

of frequency discrimination. Chapter 7 presents conclusions and suggestions for future studies.

CHAPTER 2
OVERVIEW OF SPECTRAL ANALYSIS

An important application of digital signal processing methods is in determining in the frequency content of a discrete-time signal using a process called *spectral analysis* [8]. More specifically, spectral analysis involves the determination of either the energy spectrum or the power spectrum of the signal as a function of frequency. Applications of digital spectral analysis can be found in many diverse fields. In general, spectral analysis often begins with a continuous-time signal $x(t)$ that is bandlimited, establishing what is called the Nyquist frequency and Nyquist rate. The continuous time signal is presented to a continuous-time (analog) anti-aliasing filter that limits the signal or the baseband having a maximum passband frequency limited by the Nyquist rate. The filter's output is then sampled above the Nyquist rate using a device called an analog to digital converter. The sampled or quantized sign is then presented to a spectral analysis device, such as a FFT. The resulting spectral image produced by the spectral analysis device is a facsimile of the actual frequency response of the continuous-time signal.

2.1 Spectral analysis of sinusoidal signals

Generally it is assumed that the spectral analysis of sinusoidal signals can be characterized by the sinusoidal signal's parameters amplitudes and phase for a constant frequency. For such cases the discrete Fourier transform (DFT) of a discrete time $x[n]$ is transformed into the DTFT $X(e^{j\omega})$,

where

$$X[k] = X(e^{j\omega})\Big|_{\omega=2\pi k/N}, \quad 0 \le k \le N-1 \tag{2.1}$$

In practice, the discrete-time signal *x*[*n*] maybe windowed by multiplying it with a length-*M* window *w*[*n*] to create a new *M*-sample discrete time windowed *y*[*n*] = *x*[*n*]·*w*[*n*]. The spectral characteristics of the windowed discrete time signal *y*[*n*] is obtained from its DTFT $Y(e^{j\omega})$, which is assumed to provide a reasonable estimate of the DTFT $X(e^{j\omega})$. The DTFT $Y(e^{j\omega})$ of the windowed finite-length segment *y*[*n*] is next evaluated at a set of *N* (*N* ≥ *M*) discrete angular frequencies equally spaced in the range 0 ≤ *ω* ≤ 2*π* by computing its *N*-point discrete Fourier transform (DFT) $Y[k]$. To provide sufficient resolution, the *N*-point DFT is chosen to be greater than the window *M* by zero-padding the windowed sequence with *N*-*M* zero-valued samples. The DFT is usually computed using an FFT algorithm [9].

We examine the above approach in more detail to understand its limitations so that we can properly make use of the results obtained. In particular, we analyze here the effects of windowing and the evaluation of the frequency samples of the DTFT via the DFT. Before we can interpret the spectral content of $Y(e^{j\omega})$ from $Y[k]$, we need to reexamine the relations between these transforms and their corresponding frequencies. Now, the relation between the *N*-point DFT $Y[k]$ of *y*[*n*] and its DTFT $Y(e^{j\omega})$ is given by

$$Y[k] = Y(e^{j\omega})\Big|_{\omega=2\pi k/N}, \quad 0 \le k \le N-1. \tag{2.2}$$

The normalized discrete-time angular frequency ω_k corresponding to the DFT bin number *k* (DFT frequency) is given by

$$\omega_k = \frac{2\pi k}{N}. \tag{2.3}$$

Likewise, the continuous-time angular frequency Ω_k corresponding to the DFT bin number *k* (DFT frequency) is given by

$$\Omega_k = \frac{2\pi k}{NT}. \tag{2.4}$$

To interpret the results of the DFT-based spectral analysis correctly, we first consider the frequency domain analysis of a sinusoidal sequence. Now an infinite-length sinusoidal sequence *x*[*n*] of normalized angular frequency ω_0 is given by

$$x[n] = \cos(\omega_0 n + \phi), \quad 0 \le n \le M-1. \tag{2.5}$$

By expressing the above sequence as

$$x[n] = \frac{1}{2}(e^{j(\omega_0 n+\phi)} + e^{-j(\omega_0 n+\phi)}), \tag{2.6}$$

we arrive at the expression for its DTFT as

$$X(e^{j\omega}) = \pi \sum_{l=-\infty}^{\infty} \left(e^{j\phi}\delta(\omega - \omega_0 + 2\pi l) + e^{-j\phi}\delta(\omega + \omega_0 + 2\pi l) \right). \tag{2.7}$$

Thus, the DTFT is a periodic function of ω with a period 2π containing two impulses in each period. In the frequency range, $-\pi \le \omega \le \pi$, there is an impulse at $\omega=\omega_0$ of complex amplitude $\pi e^{j\phi}$ and an impulse at $\omega=-\omega_0$ of complex amplitude $\pi e^{-j\phi}$.

To analyze *x*[*n*] in the spectral domain using the DFT, the simple example of the computation of the DFT of a finite-length sinusoid has been introduced. In this example, we computed the DFT of a length-32 sinusoid of frequency 10 Hz sampled at 64 Hz, as shown in Figure 2-1. As can be seen from this figure, there are only two nonzero DFT samples, one at bin *k* = 5 and the other at bin *k* = 27. From Eq. (2.4), bin *k* = 5 corresponds to frequency 10 Hz, while bin *k* = 27 corresponds to frequency 54 Hz, or

equivalently, -10 Hz. Thus, the DFT has correctly identified the frequency of the sinusoid.

Next, we computed the 32-point DFT of a length-32 sinusoid of frequency 11 Hz sampled at 64 Hz, as shown in Figure 2-2. This figure shows two strong peaks at bin locations k = 5 and k = 6 with nonzero DFT samples at other bin locations in the positive half of the frequency range. Note that the bin locations 5 and 6 correspond to frequencies 10 Hz and 12 Hz, respectively, according to Eq. (2.4). Thus the frequency of the sinusoid being analyzed is exactly halfway between these two bin locations.

The phenomenon of the spread of energy from a single frequency to many DFT frequency locations as demonstrated by this figure is called *spectral leakage* [10]. To understand the cause of this effect, we recall that the DFT $Y[k]$ of a length-M sequence $y[n]$ is given by the samples of its discrete-time Fourier transform (DTFT) $Y(e^{j\omega})$ evaluated at $\omega = 2\pi k/N$, k = 0, 1, ... , N-1. Figure 2-3 shows the DTFT of the length-32 sinusoidal sequence of frequency 11 Hz sampled at 64 Hz. It can be seen that the DFT samples shown in Figure 2-2 are indeed obtained by the frequency samples of the plot of Figure 2-3.

To understand the shape of the DTFT shown in Figure 2-3 we observe that the sequence of Eq. (2.5) is also translated as a windowed version of the infinite-length sequence $x[n]$ obtained using a rectangular window $w[n]$ [11]:

$$w[n] = \begin{cases} 1, & 0 \le n \le M-1, \\ 0, & \text{otherwise.} \end{cases} \tag{2.9}$$

Hence, the DTFT $Y(e^{j\omega})$ of $y[n]$ is given by the frequency-domain convolution of the DTFT $X(e^{j\omega})$ of $x[n]$ with the DTFT $\Psi_R(e^{j\omega})$ of the rectangular window $w[n]$:

$$Y(e^{j\omega}) = \frac{1}{2\pi}\int_{-\pi}^{\pi} X(e^{j\varphi})\Psi_R(e^{j(\omega-\varphi)})d\varphi\,, \tag{2.10}$$

where

$$\Psi_R(e^{j\omega}) = e^{-j\omega(M-1)/2}\,\frac{\sin(\omega M/2)}{\sin(\omega/2)}\,. \tag{2.11}$$

Substituting $X(e^{j\omega})$ from Eq. (2.7) into Eq. (2.10), we arrive at

$$Y(e^{j\omega}) = \frac{1}{2}e^{j\phi}\Psi_R(e^{j(\omega-\omega_0)}) + \frac{1}{2}e^{-j\phi}\Psi_R(e^{j(\omega+\omega_0)})\,. \tag{2.12}$$

As indicated by the above equation, the DTFT $Y(e^{j\omega})$ of the windowed sequence *y*[*n*] is a sum of the frequency shifted and amplitude scaled DTFT $\Psi_R(e^{j\omega})$ of the window *w*[*n*] with the amount of frequency shifts given by $\pm\omega_0$. Now, for the length-32 sinusoid of frequency 11 Hz sampled at 64 Hz, the normalized frequency of the sinusoid is 11/64 = 0.172. Hence, its DTFT is obtained by frequency shifting the DTFT $\Psi_R(e^{j\omega})$ of a length-32 rectangular window to the right and to the left by the amount 0.172 × *2π* = *0.344π,* adding both shifted versions, and then amplitude scaling by a factor 1/2. In the normalized angular frequency range 0 to *2π,* which is one period of the DTFT, there are two peaks, one at *0.344π* and the other at *2π* (1 - 0.172) = *1.656π,* as verified by Figure 2-3. A 32-point DFT of this DTFT is precisely the DFT shown in Figure 2-2. The two peaks of the DFT at bin locations *k* = 5 and *k* = 6 are frequency samples of the main lobe located on both sides of the peak at the normalized frequency 0.172. Likewise, the two peaks of the DFT at bin locations *k* = 26 and *k* = 27 are frequency samples of the main lobe located on both sides of the peak at the normalized frequency 0.828. All other DFT samples are given by the samples of the sidelobes of the DTFT of the window

causing the leakage of the frequency components at $\pm\omega_0$ to other bin locations with the amount of leakage determined by the relative amplitude of the main lobe and the sidelobes. Since the relative sidelobe level A_{sl}, defined by the ratio in dB of the amplitude of the main lobe to that of the largest sidelobe, of the rectangular window is very high, there is a considerable amount of leakage to the bin locations adjacent to the bins showing the peaks in Figure 2-2.

2.2 Limitations: Spectral leakage and uniform resolution

The limitation, as mentioned in the previous section, gets more complicated if the signal being analyzed has more than one sinusoid, as is typically the case. We illustrate the DFT-based spectral analysis approach by means of the next simulations. Through these simulations we examine the effects of the *N*-point DFT, the type of window being used, and its length *M* on the results of spectral analysis.

To show the limitation due to spectral leakage, we compute the various length *N* of the DFT of the two length-16 sinusoidal sequences whose frequencies are 0.22 and 0.34. Figure 2-4 (A) shows the magnitude of the DFT samples of the signal $x[n]$ for N=16. From the Figure 2-4 (A) it is difficult to determine whether there are one or more sinusoids in the signal being examined, and the exact locations of the sinusoids. To increase the accuracy of the locations of the sinusoids, we increase the size of the DFT to 32 and recomputed the DFT as indicated in Figure 2-4 (B). In this plot there appears to be some concentrations around k=7 and around k=11 in the normalized frequency range from 0 to 0.5. Figure 2-4 (C) shows the DFT plot obtained for N=24. In this plot there are two clear peaks occurring at k=13 and k=22 that correspond to the normalized frequencies of 0.2031 and 0.3438, respectively. To improve further the accuracy of the

peak location, we compute next a 128-point DFT as shown in Figure2-4 (D) in which the peak occurs around k=27 and k=45 corresponding to the normalized frequencies of 0.2109 and 0.3516, respectively. However, this plot also shows a number of minor peaks, and it is not clear by examining this DFT plot whether additional sinusoids of lesser strengths are present in the original signal or not. As this simulations point out, in fact, an increase in the DFT length improves the sampling accuracy of the DTFT by reducing the spectral separation of adjacent DFT samples. But it also increases the computational complexity and thereby reduces the real-time capabilities of the system

The other limitation is the uniform resolution. In general, the DFT provides a uniform frequency resolution given by $\Delta = 2\pi/N$ over the normalized baseband, $-\pi \leq \omega \leq \pi$. The DFT's frequency resolution Δ is uniform across the baseband. This fact historically has limited the role of the DFT in performing acoustic and modal (vibration) signal analysis applications. These application areas prefer to interpret a signal spectrum in the context of logarithmic (octave) frequency dispersion. Another application area in which a fixed frequency resolution is a limiting factor is multi-tone signal detection and classification. It is generally assumed that if two tones are separated by 1.6 Δ (1.6 harmonics) or less, then a uniformly windowed DFT/FFT cannot determine if one tone or multiple tones are present locally about a harmonic frequency. To show this limitation, we compute the DFT of a sum of two finite-length sinusoidal sequences with one of the sinusoids at a fixed frequency, while the frequency of the other sinusoid is varied. Specifically, we keep one frequency 0.34 and vary the other frequency from 0.28 to 0.31. Figure 2-5 shows the plots of the 256-point DFT computed, along with the frequencies of the sinusoids. As can be seen from these plots, the two sinusoids are clearly resolved

in Figure 2-5 (A) and (B), while they cannot be resolved in Figure 2-5 (C) and (D) as the frequencies are closer to each other. The reduced resolution occurs when the difference between the two frequencies becomes less than 0.04.

In the case of a sum of two length-M sinusoids of normalized angular frequencies ω_1 and ω_2, the DTFT is obtained by summing the DTFTs of the individual sinusoids. As the difference between the two frequencies becomes smaller, the main lobes of the DTFTs of the individual sinusoids get closer and eventually overlap. If there is a significant overlap, it will be difficult to resolve the peaks. It follows therefore that the frequency resolution is essentially determined by the width Δ_{ML} of the main lobe of the DTFT of the window. The main lobe width Δ_{ML} of a length-M rectangular window is given by $4\pi/M$ from Table 2-1 [12]. In terms of normalized frequency, the main lobe width of a length-16 rectangular window is 0.125. Hence, two closely spaced sinusoids windowed with a rectangular window of length 16 can be clearly resolved if the difference in their frequencies is about half of the main lobe width, i.e., 0.0625. Even though the rectangular window has the smallest main lobe width, it has the largest relative sidelobe amplitude and, as a consequence, causes considerable leakage. So the large amount of leakage results in minor peaks that may be falsely identified as sinusoids as shown in Figure 2-4 and 2-5.

As a result, the performance of the DFT-based spectral analysis depends on several factors, the type of window being used and its length, and the size (N) of the DFT. To improve the frequency resolution, one must use a window with a very small main lobe width, and to reduce the leakage, the window must have a very small relative sidelobe level. The main lobe width can be reduced by increasing the length of the

window. Furthermore, an increase in the accuracy of locating the peaks is achieved by increasing the size of the DFT. To this end, it is preferable to use a DFT length that is a power of 2 so that very efficient FFT algorithms can be employed to compute the DFT. An increase in the DFT size, however, also increases the computational complexity of the spectral analysis procedure which causes cost penalty. Therefore, to resolve two or more tones without increasing the DFT size the WDFT is introduced as an alternative to spectral analysis in the next chapter.

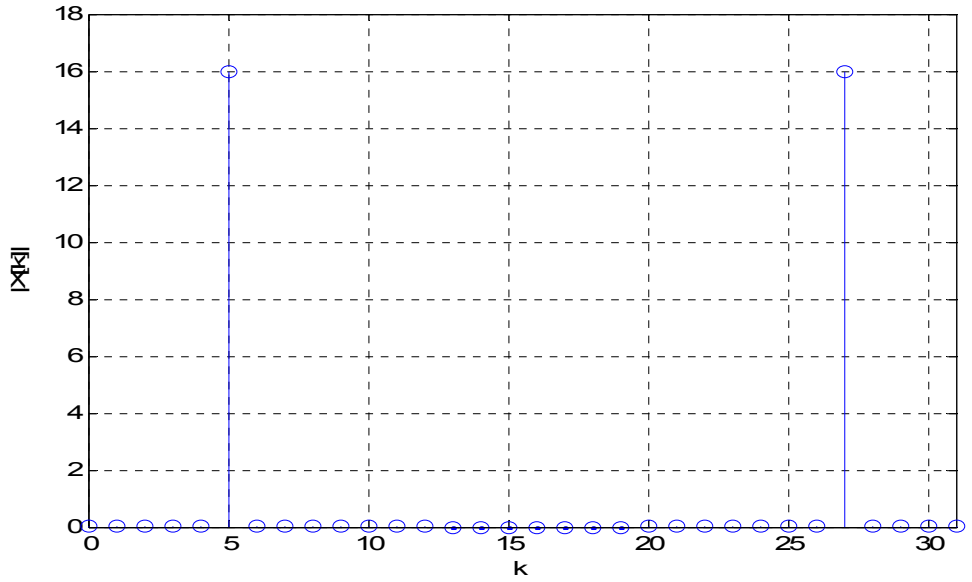

Figure 2-1. Magnitude of a 32-point DFT of a sinusoid of frequency 10 Hz sampled at a 64-Hz rate

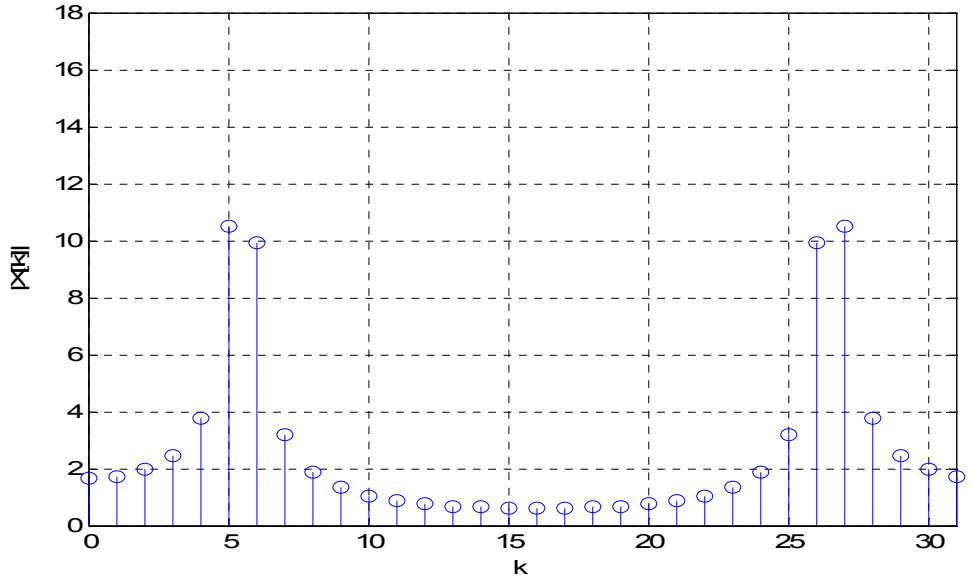

Figure 2-2. Magnitude of a 32-point DFT of a sinusoid of frequency 11 Hz sampled at a 64-Hz rate.

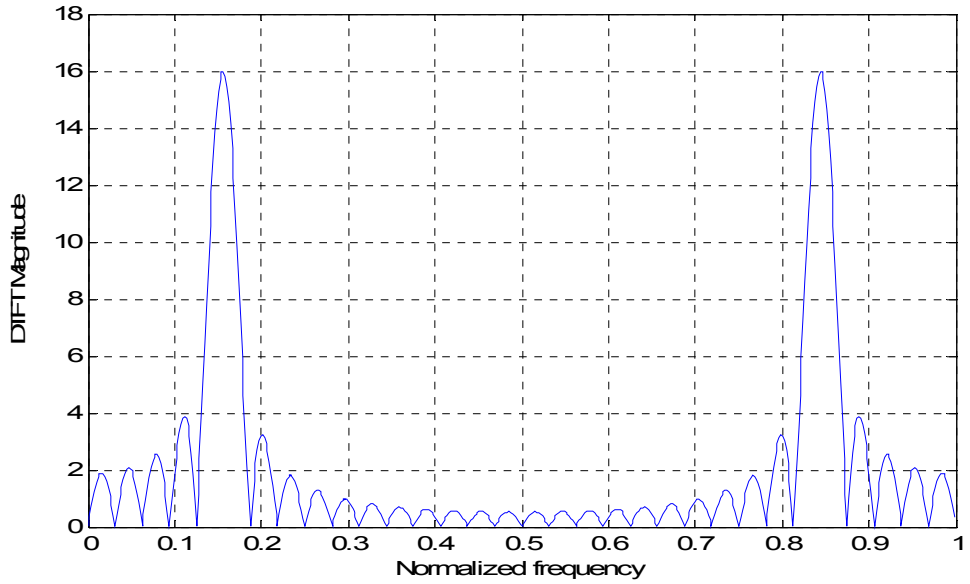

Figure 2-3. DTFT of a sinusoid sequence windowed by a rectangular window.

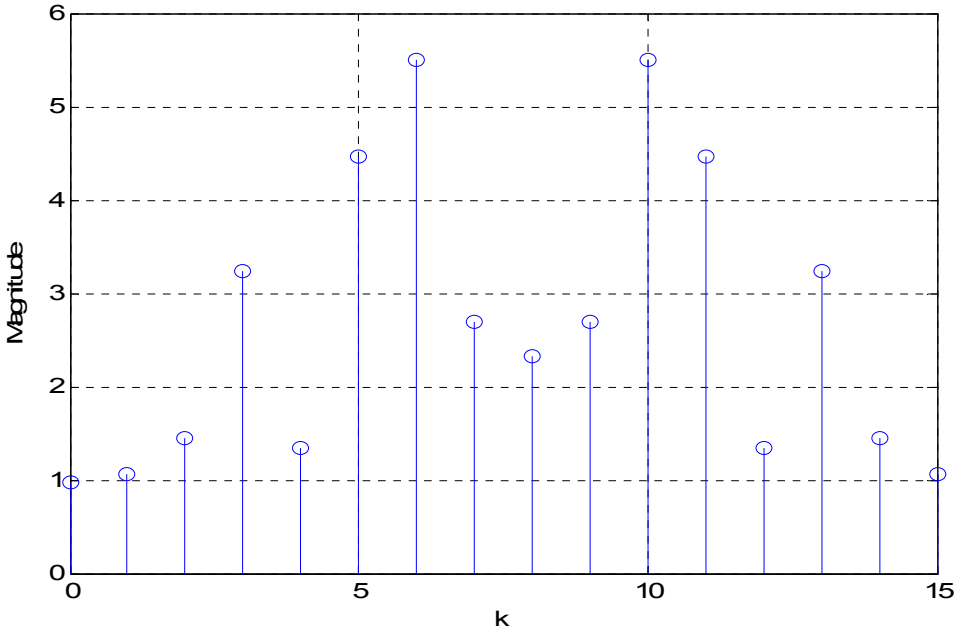

A

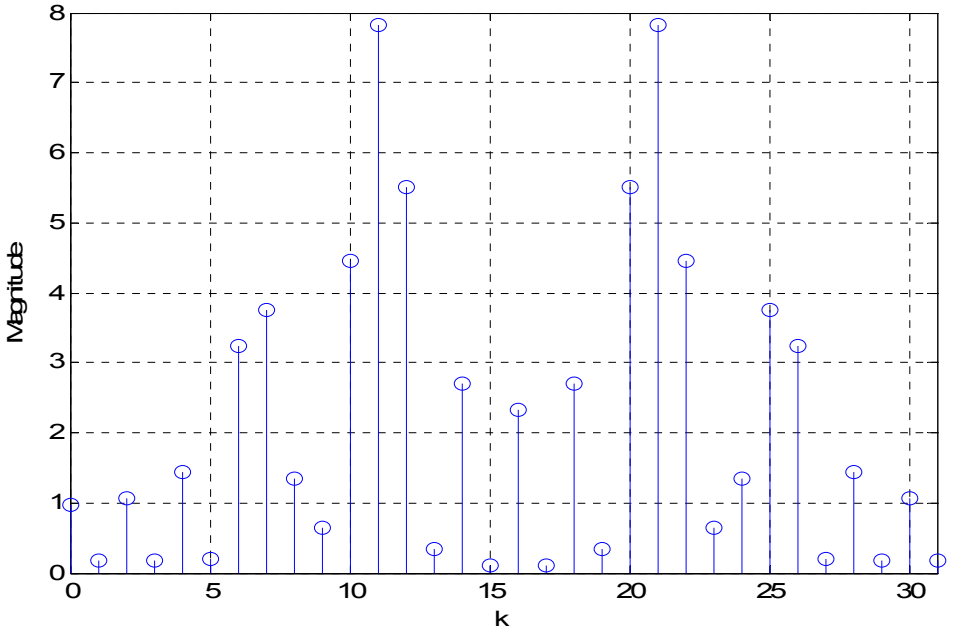

B

Figure 2-4. DFT-based spectral analysis of a sum of two finite-length sinusoidal sequences of normalized frequencies 0.22 and 0.34, respectively, of length 16 each for A)N=16, B)N=32, C)N=64, and D)N=128 of DFT length.

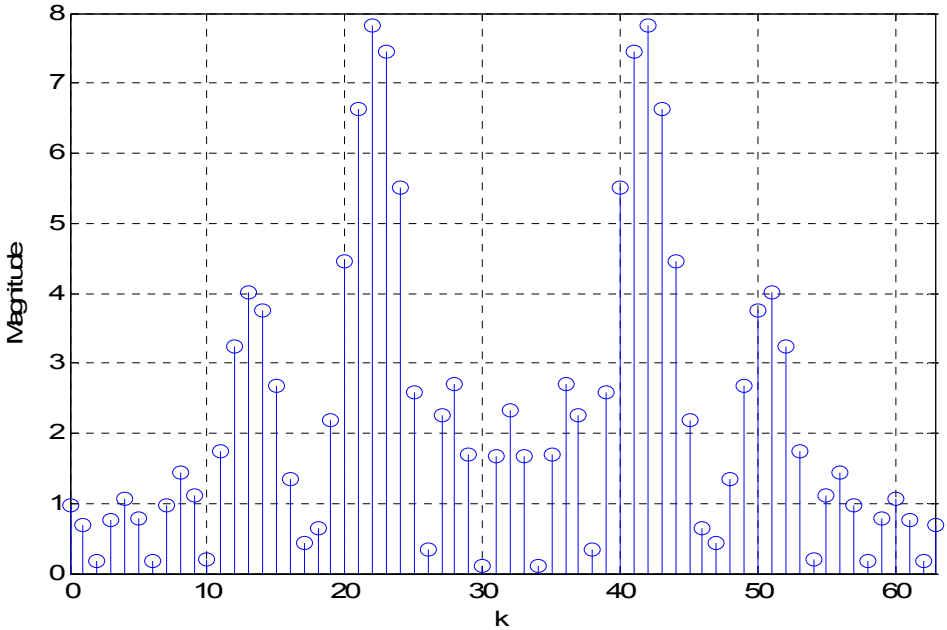

C

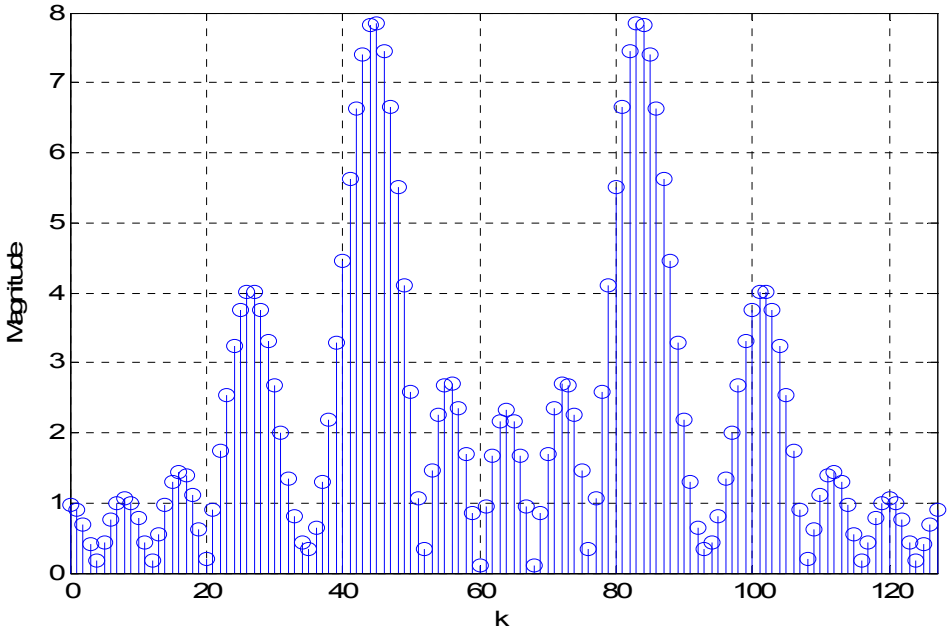

D

Figure 2-4. Continued

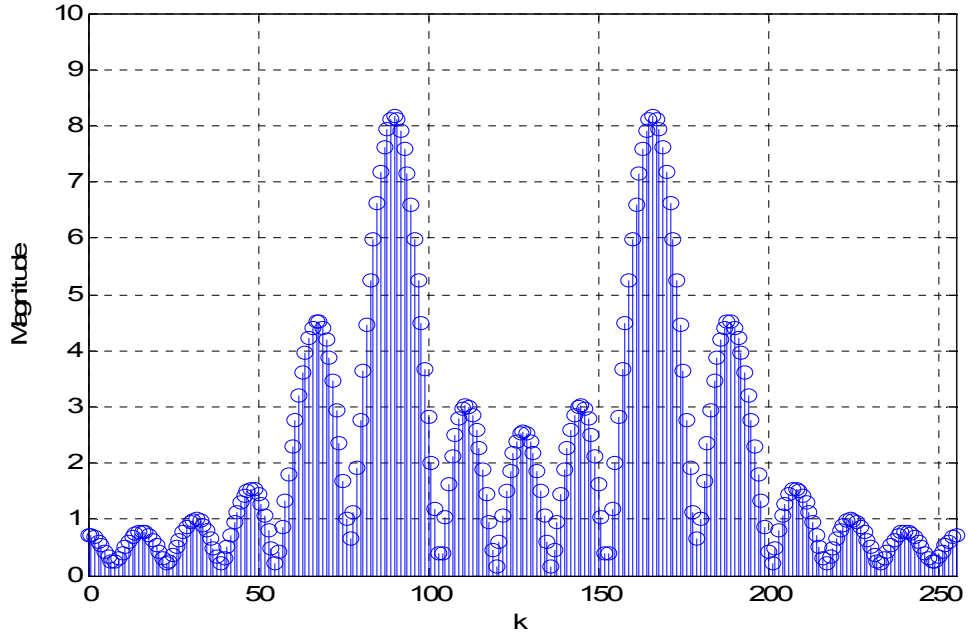

A

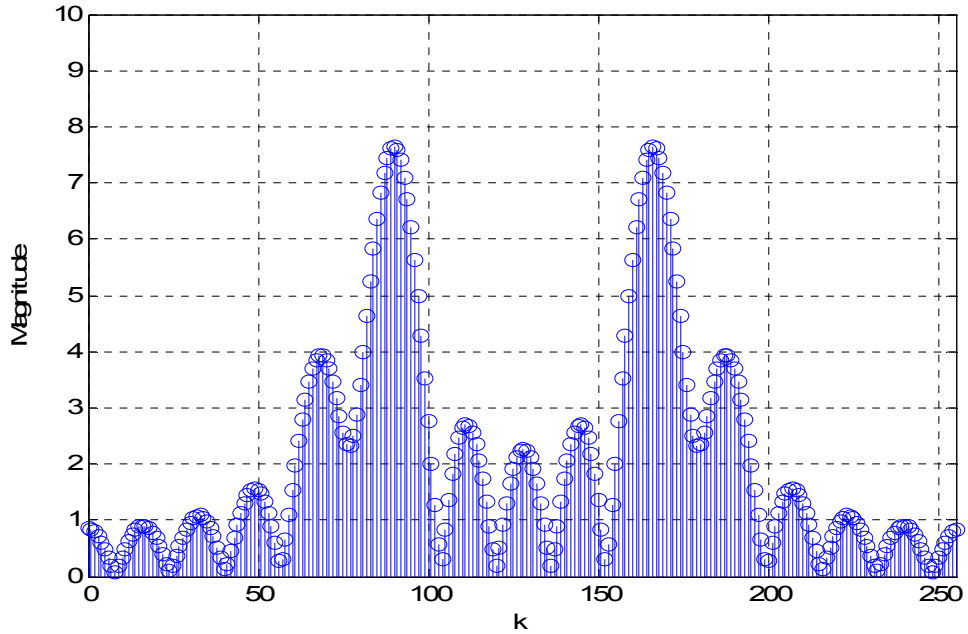

B

Figure 2-5. Example of two tones separated between A) f_1 = 0.28 and f_2 = 0.34, B) f_1 = 0.29 and f_2 = 0.34, C) f_1 = 0.3 and f_2 = 0.34, and D) f_1 = 0.31 and f_2 = 0.34 with 256-point DFT.

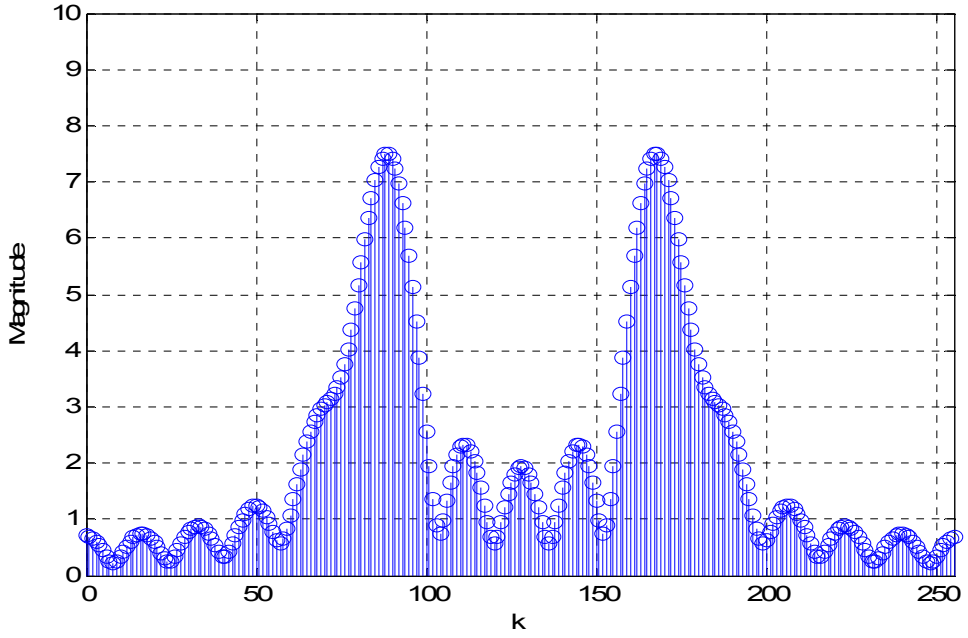

C

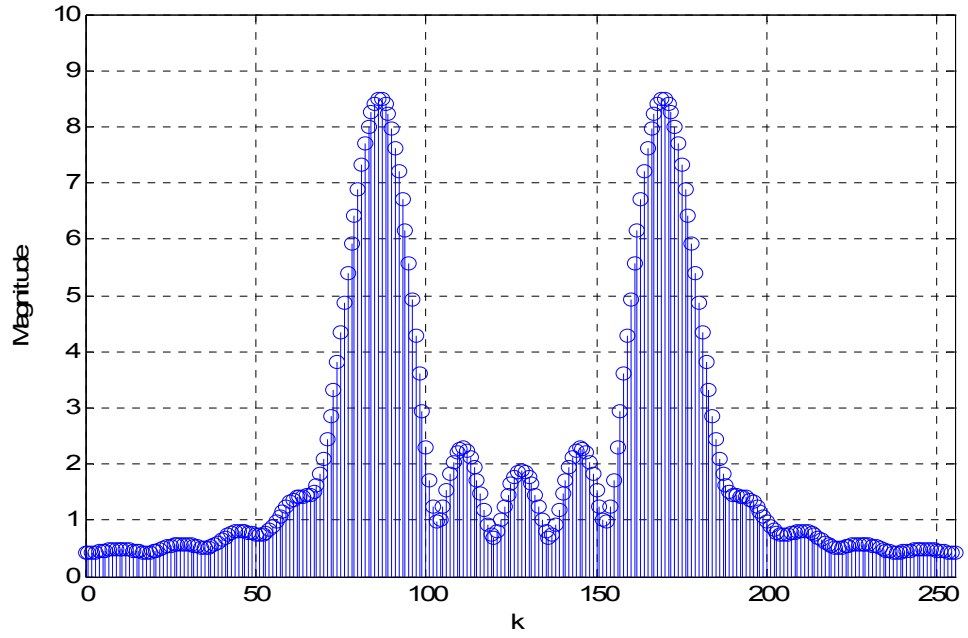

D

Figure 2-5. Continued

Table 2-1. Properties of some fixed window functions

Type of window	Main lobe width Δ_{ML}	Relative sidelobe level A_{sl}	Min. stopband attenuation	Transition bandwidth Δ_{ω}
Rectangular	$4\pi/(2M+1)$	13.3 dB	20.9 dB	$0.92\pi / M$
Hann	$8\pi/(2M+1)$	31.5 dB	43.9 dB	$3.11\ \pi / M$
Hamming	$8\pi/(2M+1)$	42.7 dB	54.5 dB	$3.32\ \pi / M$
Blackman	$12\pi/(2M+1)$	58.1 dB	75.3 dB	$5.56\ \pi / M$

CHAPTER 3
TRANSFORMS FOR SIGNAL ANALYSIS

3.1 Discrete Fourier Transform (DFT)

The venerable discrete Fourier transform (DFT) is an important signal analysis tool. Generally, the preferred instantiation of the DFT is the Cooley-Tukey fast Fourier transform (FFT) algorithm. An *N*-point DFT *X*[*k*], for 0≤*k*≤*N*-1, of a length-*N* time-series *x*[*n*], for 0≤*n*≤*N*-1, is defined by:

$$X[k] = \sum_{n=0}^{N-1} x[n] e^{-j2\pi kn/N},\ 0 \le k \le N-1 \tag{3.1}$$

Note that *X*[*k*] is a length *N* sequence of complex harmonics corresponding to *N*/2 positive harmonics and *N*/2 negative harmonics. Using the so-called "*W*" notation ($W_N = e^{-j2\pi/N}$), equation (3.1) can be rewritten as:

$$X[k] = \sum_{n=0}^{N-1} x[n] W_N^{kn},\ 0 \le k \le N-1. \tag{3.2}$$

The inverse discrete Fourier transform (IDFT) is given by:

$$x[n] = \frac{1}{N} \sum_{k=0}^{N-1} X[k] W_N^{-kn},\ 0 \le n \le N-1. \tag{3.3}$$

There are applications where it is desirable to compute the frequency components of a finite-length sequence having unequal or non-uniform frequency resolution. To this end, Oppenheim and Johnson proposed transformation $x[n]$ into a new sequence $y[n]$ by means of an allpass network [13]. The magnitude of the frequency components of $Y(z)$, the *z*-transform $y[n]$, is equally-spaced points on the periphery of unit circle in the z-domain. Since the allpass network has an IIR transfer function, $y[n]$ is an infinite-length sequence and hence, must be made into a finite-length sequence by using an

appropriate window function before its DFT can be computed. Figure 3-1 shows their scheme. Moreover, the initial conditions of the IIR allpass network will propagate to the output. As a result, this scheme provides an approximate estimate of the magnitudes of the DFT of $x[n]$ at unequal resolutions.

3.2 Non-uniform Discrete Fourier Transform (NDFT)

The non-uniform DFT (NDFT) [14] is the most general form of DFT that can be employed to evaluate the frequency components of $X(z)$ at *N* arbitrary but distinct points in *z*-plane. If z_k, $0 \le k \le N-1$, denote *N* distinct frequency points in the *z*-plane, the *N*-point NDFT of the length- *N* sequence $x[n]$ is then given by

$$X_{NDFT}[k] = X(z_k) = \sum_{n=0}^{N-1} x[n] z_k^{-n}, \quad 0 \le k \le N-1. \tag{3.4}$$

In matrix form, the above *N* equations can be written in the form

$$\begin{bmatrix} X_{NDFT}[0] \\ X_{NDFT}[1] \\ \vdots \\ X_{NDFT}[N-1] \end{bmatrix} = \mathbf{D}_N \cdot \begin{bmatrix} x[0] \\ x[1] \\ \vdots \\ x[N-1] \end{bmatrix} \tag{3.5}$$

where $\mathbf{D}_N$ is the $N \times N$ NDFT matrix given by

$$\mathbf{D}_N = \begin{bmatrix} 1 & z_0^{-1} & \cdots & z_0^{-N+1} \\ 1 & z_1^{-1} & \cdots & z_1^{-N+1} \\ \vdots & \vdots & & \vdots \\ 1 & z_{N-1}^{-1} & \cdots & z_{N-1}^{-N+1} \end{bmatrix} \tag{3.6}$$

where $\mathbf{D}_N$ is a Van der Monde matrix and is invertible if the points z_k are distinct. In general, the computation of an NDFT involves the multiplication of the NDFT matrix $\mathbf{D}_N$

with the length-*N* vector composed of sample values of $x[n]$ resulting in an algorithm of complexity O(N^2), i.e.,N^2 complex multiplications.

The NDFT computation can be made computationally efficient by imposing some restrictions on the locations of the points z_k in the *z* domain. For example, if the points are located equidistant on the unit circle at $z_k = e^{j2\pi k/N}$, then the NDFT reduces to the conventional DFT which can be computed very efficiently using fast Fourier transform (FFT) algorithms. Note that the resolution of the DFT depends on the spacing between frequency points. An increase in frequency resolution can be obtained by increasing the DFT length. However, an increase in the DFT length also increases the computational complexity.

In this dissertation, we consider an alternate structure to the location of the frequency points z_k by applying an allpass transformation to warp the frequency axis. Then, uniformly spaced points on the warped frequency axis are equivalent to a non-uniform spacing frequency points on the original frequency axis. This has led to the concept of the warped DFT (WDFT) which evaluates the frequency signature of *x*[*n*] at unequally spaced points (frequencies) on the unit circle. By choosing a control variable called the warping parameter, the WDFT can more densely space some of frequency and sparsely distribute frequency points elsewhere reducing spectral precision without increasing the DFT length. An efficient realization of the WDFT is also proposed that can implement a WDFT.

3.3 Warped Discrete Fourier Transform (WDFT)

A. Definition and properties

The WDFT is a derivative of the familiar DFT. The DFT is designed to evaluate a signal at frequencies that are uniformly distributed along the periphery of the unit-circle in the *z*-domain at locations $z = e^{-j2\pi k/N}$. Unlike the DFT, the WDFT evaluates a signal at non-uniformly distributed locations on the periphery of the unit circle in the z-domain (i.e., critical frequencies). More specifically, an *N*-point WDFT, denoted $\overline{X}[k]$, of a length-*N* time-series $x[n]$ is a modified *z*-transform $\overline{X}(z)$ obtained from $X(z)$ by applying the transformation:

$$z^{-1} \leftarrow A(z) \tag{3.7}$$

where $A(z)$ is an Mth-order real coefficient all-pass filter function. The all-pass transformation warps the frequency axis and thereby associates uniformly spaced points on the unit circle with their non-uniformly-spaced counterparts in the *z*-plane.

Applying the mapping of equation (3.7) to:

$$X(z) = \sum_{n=0}^{N-1} x[n] z^{-n} , \tag{3.8}$$

one obtains:

$$\overline{X}[k] = \overline{X}(z)\Big|_{z=e^{j\omega}} = \sum_{n=0}^{N-1} x[n] A(z)^n \Big|_{z=e^{j\omega}} . \tag{3.9}$$

Using matrix notation, the above equation can be written in the form:

$$\overline{X} = \mathbf{D}_{\text{WDFT}} \cdot \mathrm{x} \tag{3.10}$$

where x=[x[0],x[1],…,x[N-1]]^{T} is the vector of the input time sequence, and $\mathbf{D}_{\text{WDFT}}$ is the complex *N*×*N* WDFT matrix given by:

$$\mathbf{D}_{\mathrm{WDFT}} = \begin{bmatrix} 1 & 1 & \mathrm{K} & 1 \\ 1 & A(W_N^1)^1 & \mathrm{K} & A(W_N^1)^{N-1} \\ \mathrm{M} & \mathrm{M} & & \mathrm{M} \\ 1 & A(W_N^{N-1})^1 & \mathrm{K} & A(W_N^{N-1})^{N-1} \end{bmatrix}. \tag{3.11}$$

Many, but not all, of the well known DFT properties such as linearity, periodicity, time or frequency shifting, symmetries etc., also hold for WDFT. A few key properties are reported in Table 3-1.

B. Realization

To realize the WDFT, we denote from equation (3.7)

$$A(z) = \frac{\overline{A}(z)}{A(z)} \tag{3.12}$$

where $A(z)$ is the mirror-image polynomial of $\overline{A}(z)$, (i.e., $\Pi(z) = z^{-M}\Pi(z^{-1})$), resulting in

$$\overline{X}(z) = \sum_{n=0}^{N-1} x[n]\left[\frac{\overline{A}(z)}{A(z)}\right]^n = \frac{P_e(z)}{D_e(z)} \tag{3.13}$$

where,

$$P_e(z) = \sum_{n=0}^{N-1} x[n]A^{N-1-n}(z)\overline{A}(z) \tag{3.14}$$

$P_e(z)$ is a polynomial of degree *M(N-1)* that is a function of $x[n]$ and

$$D_e(z) = A^{N-1}(z) \tag{3.15}$$

is another polynomial of degree *M(N-1)* that is not a function of $x[n]$.

WDFT is defined as $\overline{X}(z)$ evaluated at $z = e^{j2\pi k/N}$

$$\overline{X}[k] = \overline{X}(z)\Big|_{z=e^{j2\pi k/N}} = \frac{P_e(z)\big|_{z=e^{j2\pi k/N}}}{D_e(z)\big|_{z=e^{j2\pi k/N}}} \tag{3.16}$$

To simplify equation (3.16), we define

$$P(z) = P_e(z) \bmod z^N$$
$$= \sum_{n=0}^{N-1} \left[\sum_{m \geq 0, n+mN \leq M(N-1)} p_{e_{n+mN}} \right] z^{-n} \tag{3.17}$$

where p_{e_i} is the *ith coefficient of* $P_e(z)$ and

$$D(z) = D_e(z) \bmod z^N . \tag{3.18}$$

$P(z)$ and $D(z)$ both have degree *N*-1. So the WDFT computation as shown in equation (3.16) is simplified to

$$\overline{X}[k] = \frac{P(z)\big|_{z=e^{j2\pi k/N}}}{D(z)\big|_{z=e^{j2\pi k/N}}} . \tag{3.19}$$

Let $\overline{P}[k]$ and $\overline{D}[k]$ be the *N*-point DFT of the length *N* sequences obtained from the co efficients of $P(z)$ and $D(z)$

$$\overline{P}[k] = \overline{P}(z)\Big|_{z=e^{j2\pi k/N}} , \ \overline{D}[k] = \overline{D}(z)\Big|_{z=e^{j2\pi k/N}} \tag{3.20}$$

Then we obtain

$$\overline{X}(z) = \frac{\overline{P}(z)}{\overline{D}(z)} \tag{3.21}$$

Using matrix notation, we can define $\mathbf{P}$ as

$$\mathbf{P} = \mathbf{Q} \cdot \mathbf{x} \tag{3.22}$$

where $\mathbf{P}$ is the column vector formed by the coefficients of $\overline{P}(z)$ and $\mathbf{Q}$ is an *N*×*N* real matrix .Further, $\overline{P}[k]$ is obtained as

$$\begin{bmatrix} \overline{P}[0] \\ \overline{P}[1] \\ \vdots \\ \overline{P}[N-1] \end{bmatrix} = \mathbf{W} \cdot \mathbf{Q} \cdot \mathbf{x} \tag{3.23}$$

where $\mathbf{W}$ is the *N*×*N* DFT matrix. Finally, the WDFT coefficients are obtained as follows.

$$\begin{bmatrix} \overline{X}[0] \\ \overline{X}[1] \\ \vdots \\ \overline{X}[N-1] \end{bmatrix} = \mathbf{\Lambda_D} \cdot \mathbf{W} \cdot \mathbf{Q} \cdot \mathbf{x} \tag{3.24}$$

where

$$\mathbf{\Lambda_D} = \begin{bmatrix} \frac{1}{\overline{\overline{D}}[0]} & 0 & \cdots & 0 \\ 0 & \frac{1}{\overline{\overline{D}}[1]} & \cdots & 0 \\ \vdots & \vdots & & \vdots \\ 0 & 0 & \cdots & \frac{1}{\overline{\overline{D}}[N-1]} \end{bmatrix}. \tag{3.25}$$

Therefore, we obtain a factorization of the WDFT matrix into the product of a diagonal matrix, the DFT matrix, and a real matrix. This realization of the WDFT, which follows directly from equation (3.24), is shown in Figure 3-2.

C. Complexity

Let x be an N-dimensional complex input vector. Direct computation of the WDFT coefficients from **x** requires multiplying **x** by an $N \times N$ complex matrix, or $4N^2$ real multiplications and $4N^2$-$2N$ real additions (assuming that one complex multiplication involves four real multiplications and two real additions, and one complex addition involves two real additions). Using a reported factorization of the WDFT matrix [15], the total requirement is $N(N+2\log_2 N+4)$ real multiplications and $N(2N+3\log_2 N)$ real additions while $2N\log_2 N$ real multiplications and $3N\log_2 N$ real additions for the N-point DFT with the above assumption. Table 3-2 shows the required number of operations for some typical values of N.

D. Inverse WDFT

An inverse $\mathbf{D}_{\mathrm{WDFT}}$ equation (3.11) can be computed with the complexity of the WDFT. Unfortunately, in certain instances the condition number of $\mathbf{D}_{\mathrm{WDFT}}$ can easily exceed 10^{12} for transform lengths *N* above 50. Therefore an exact computation of an inverse WDFT can be compromised due to numerical instability. In order to stabilize the matrix inversion, we propose to compute a pseudo-inverse of a $\mathbf{D}_{\mathrm{WDFT}}$ by employing only the *r* largest singular values $\sigma_i > \varepsilon$ into inversion process [16]. In such cases the inverse WDFT can be expressed as:

$$\bar{\mathbf{x}} \approx \sum_{i=1}^{r} \frac{1}{\sigma_i} \mathbf{v}_i \mathbf{u}_i^H \cdot \mathbf{X} . \tag{3.27}$$

Using the pseudo-inverse, one can obtain

$$\Delta\mathbf{x} = \sum_{i=1}^{r} \frac{\mathbf{u}_i^H \Delta\mathbf{X}}{\sigma_i} \mathbf{v}_i . \tag{3.28}$$

The l_2 norm of the error-vector can then be estimated by:

$$\|\Delta\mathbf{x}\|_2^2 = \left\| \sum_{i=1}^{r} \frac{1}{\sigma_i} \mathbf{u}_i^H \Delta\mathbf{X} \mathbf{v}_i \right\|_2^2 \le \sum_{i=1}^{r} \frac{1}{\sigma_i^2} \left\| \mathbf{u}_i^H \right\|_2^2 \|\Delta\mathbf{X}\|_2^2 \|\mathbf{v}_i\|_2^2 = \sum_{i=1}^{r} \frac{1}{\sigma_i^2} \|\Delta\mathbf{X}\|_2^2 , \tag{3.29}$$

with $\|\mathbf{v}_i\|_2^2 = 1$ and $\|\mathbf{u}_i\|_2^2 = 1$. Equation (3.11) shows that a high error amplification is possible due to the large condition number of the $\mathbf{D}_{\mathrm{WDFT}}$ matrix (the smallest singular value is dominant). In the case of a conventional DFT, such an effect would not be present because the condition number of the $\mathbf{D}_{\mathrm{WDFT}}$ matrix is equal to 1. The limit ε evokes only a small signal distortion but makes the matrix inversion unstable. A high ε results in a stable matrix inversion but is associated with signal distortions, which can be

considered as a ‘filtering’ effect. We have observed that neglecting small singular values mostly affects the interpretation of the high frequency components of the spectra.

To obtain an efficient computation of inverse WDFT, the factorization of the WDFT matrix in equation (3.24) can be used. Assuming the frequency samples of the WDFT to be distinct, the inverse WDFT is given by

$$\mathbf{x} = \mathbf{Q}^{-1} \cdot \mathbf{W}^{-1} \cdot \mathbf{\Lambda}_{\mathbf{D}}^{-1} \cdot \begin{bmatrix} \overline{X}[0] \\ \overline{X}[1] \\ \vdots \\ \overline{X}[N-1] \end{bmatrix} \tag{3.30}$$

where $\mathbf{W}^{-1}$ is the $N \times N$ IDFT matrix. Since the rows of $\mathbf{Q}$ are mirror image pairs or symmetric, $\mathbf{Q}^{-1}$ is a matrix with real coefficients whose columns are mirror image pairs or symmetric. With an appropriate column permutation, its rows can be made mirror image pairs or symmetric. Therefore, $\mathbf{Q}^{-1}$ can be written as a $\mathbf{Q}$-like matrix post-multiplied by a permutation matrix. Consequently, the computation of an *N*-point inverse WDFT is equivalent to that of an *N*-point WDFT with an additional permutation involving no multiplication.

Figure 3-1. Scheme for computing the magnitude spectrum with unequal resolution using the FFT.

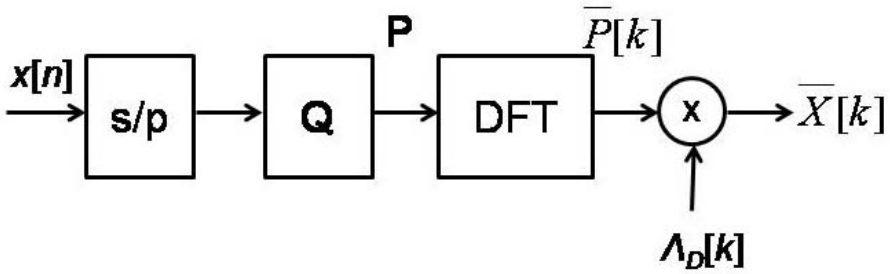

Figure 3-2. WDFT realization

Table 3-1. Some properties of the WDFT

Property	Function	WDFT
Conjugate symmetry	x[n] real	X[N-k]=X*[k]
Conjugation	x*[n]	X*[N-k]

Table 3-2. Comparison of number of operations

N	DFT		WDFT	
	real multiplication	real addition	real multiplication	real addition
4	64	56	48	56
8	256	240	144	200
16	1024	992	448	704

CHAPTER 4
WDFT USING FIRST-ORDER ALLPASS FILTER

4.1 Warping Parameter Cases Using First-Order Allpass filter

As noted in Chapter 3, the WDFT is defined in terms of an allpass filter. The allpass mapping includes a control parameter a, called the *warping parameter*. To explain the warping parameter, a simple motivational example is presented using a first-order allpass filter

$$A(z) = \frac{-a + z^{-1}}{1 - az^{-1}}. \tag{4.1}$$

The warping parameter a is real and $|a|<1$ for stability [17]. To showcase the warping parameter cases, it may be recalled that the standard z-transform of an *N* sample input time series *x*[*n*], is given by:

$$X(z) = \sum_{n=0}^{N} x[n] z^{-n}. \tag{4.2}$$

From the *X*(*z*), the conventional DFT of *x*[*n*] is obtained by:

$$X[k] = X(z)\big|_{z=e^{j2\pi k/N}},\ 0 \le k \le N-1 \tag{4.3}$$

where $e^{j2\pi k/N}$ evaluates *X*(*z*) at uniformly distributed points located on the periphery of the unit circle in the *z*-domain.

Referring to equation (3.9) and replacing z^{-1} with equation (4.1), then $\overline{X}(z)$ is given by:

$$\overline{X}(z) = \sum_{n=0}^{N} x[n] \left(\frac{-a + z^{-1}}{1 - az^{-1}} \right)^{n}. \tag{4.4}$$

The WDFT coefficient, then, $\overline{X}[k]$ are similarly obtained by sampling $\overline{X}(z)$ at non-uniform points on the periphery of the unit circle in the *z*-domain, namely

$$\overline{X}[k] = \overline{X}(z)\Big|_{z=e^{j2\pi k/N}},\ 0 \le k \le N-1 \quad (4.5)$$

A conventional uniform frequency resolution DFT, defined by $z = e^{j\omega}$, has harmonic frequencies uniformly located at frequencies at $\omega_k = 2\pi k / N$. The center frequencies of an *N* point WDFT spectrum are located at the warped frequencies $\overline{\omega}$ (to differentiate them from ω), where $z = e^{j\overline{\omega}}$. The frequencies $\overline{\omega}$ are related to ω through the nonlinear frequency warping relationship

$$\overline{\omega} = 2\arctan\left(\frac{1+a}{1-a}\right)\tan\left(\frac{\omega}{2}\right). \quad (4.6)$$

Equation (4.6) establishes a non-linear frequency warping relationship that is controlled by the real parameter a. The conventional DFT becomes a special case of the WDFT when a=0. The frequency warping property of equation (4.6) is graphically illustrated in Figure 4-1 over a range of *a*. A positive a provides higher frequency resolution on the high frequency baseband region. A negative value of a increases frequency resolution in the low frequency baseband region. Figure 4-2 illustrates the non-uniform sampling of the WDFT by showing the location of samples on the unit circle of the *z* plane for the DFT and the WDFT for *N*=32.

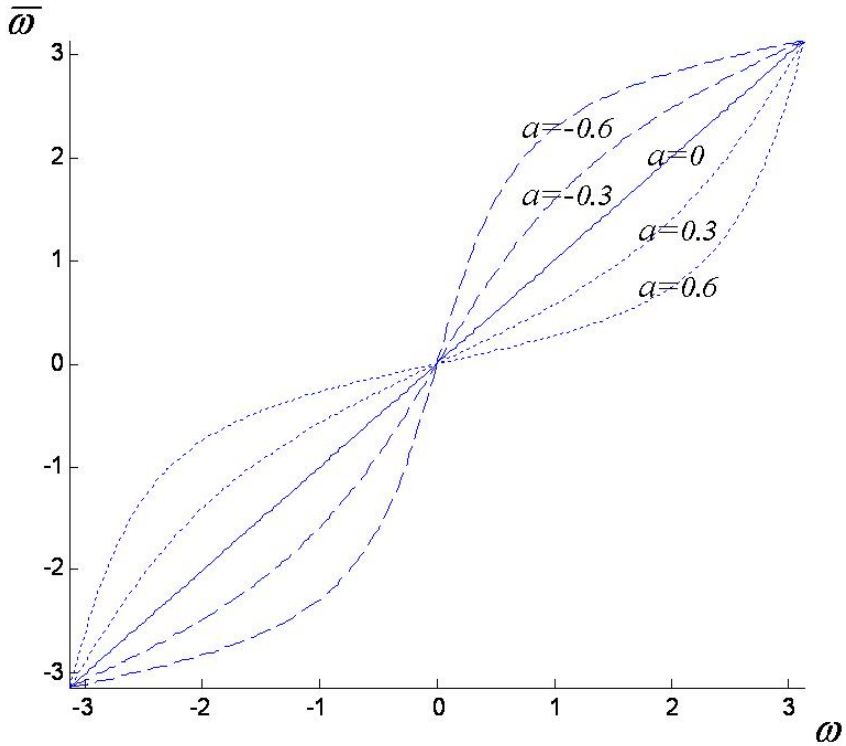

Figure 4-1. Frequency mapping

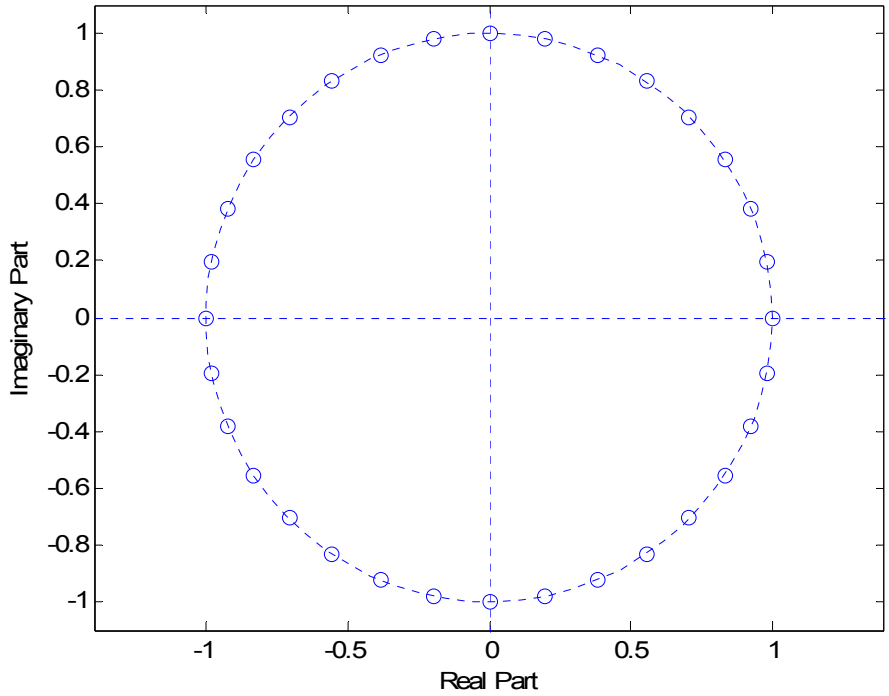

A

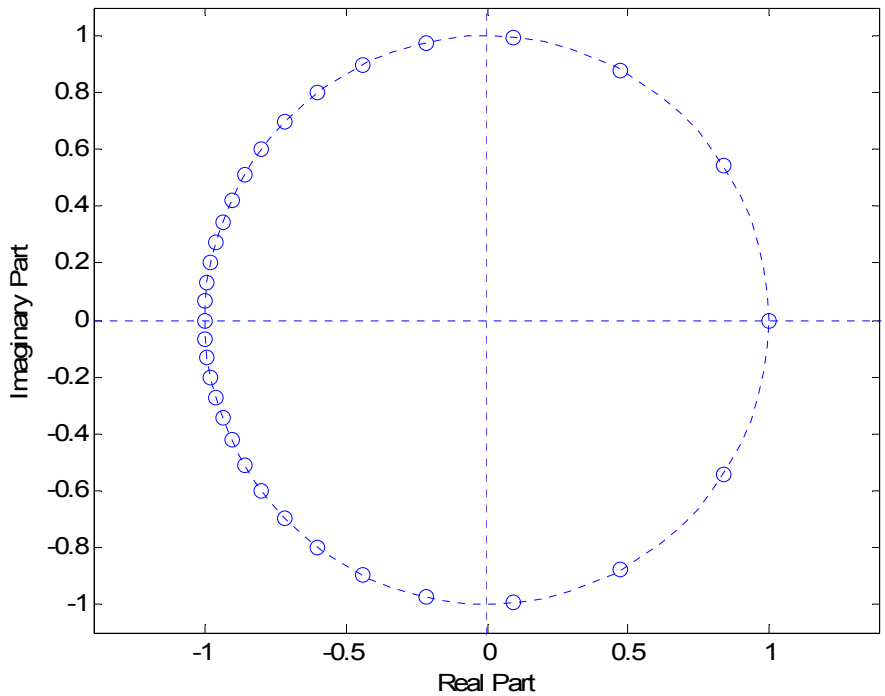

B

Figure 4-2. Location of frequency samples for DFT and WDFT for N=32 with A).a = 0, B) a=0.5 and C) a=-0.5.

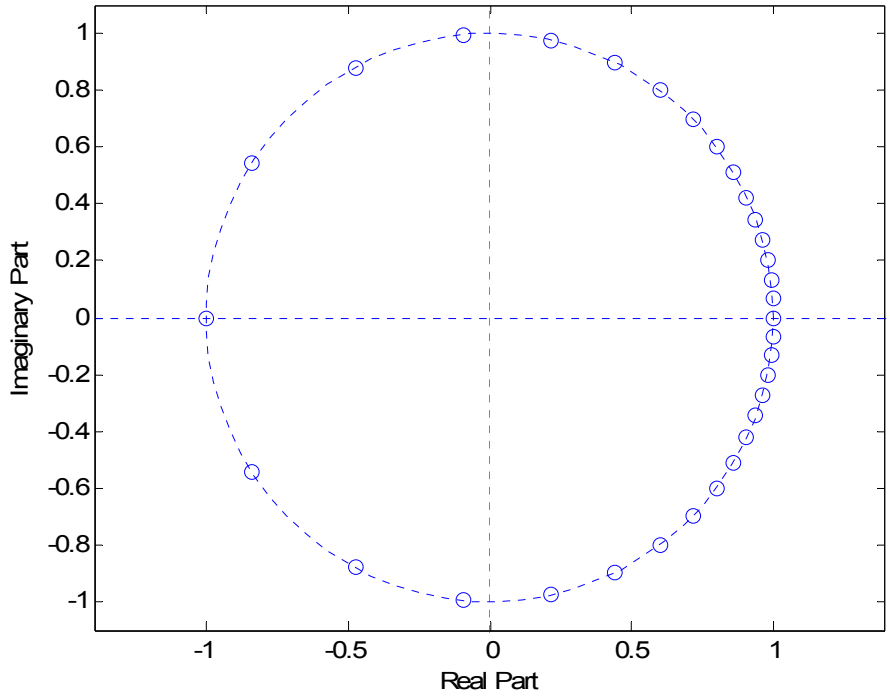

C

Figure 4-2. Continued

4.2 MATLB Simulation

The WDFT ($|a| < 1.0$) is compared to the DFT (a=0) in Figure 4-3. Observe that the frequency resolution is compressed as a decreases. This property can be used to perform non-uniform frequency discrimination.

A

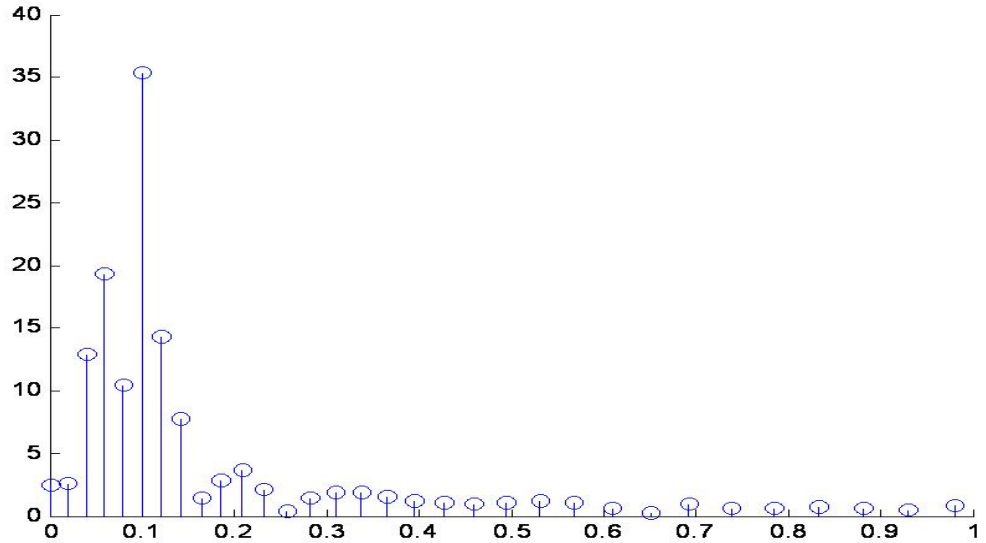

B

Figure 4-3. Magnitude spectrum for two tones with 64 point WDFT for A) a = 0, B) a = -0.23, and C) a = -0.4.

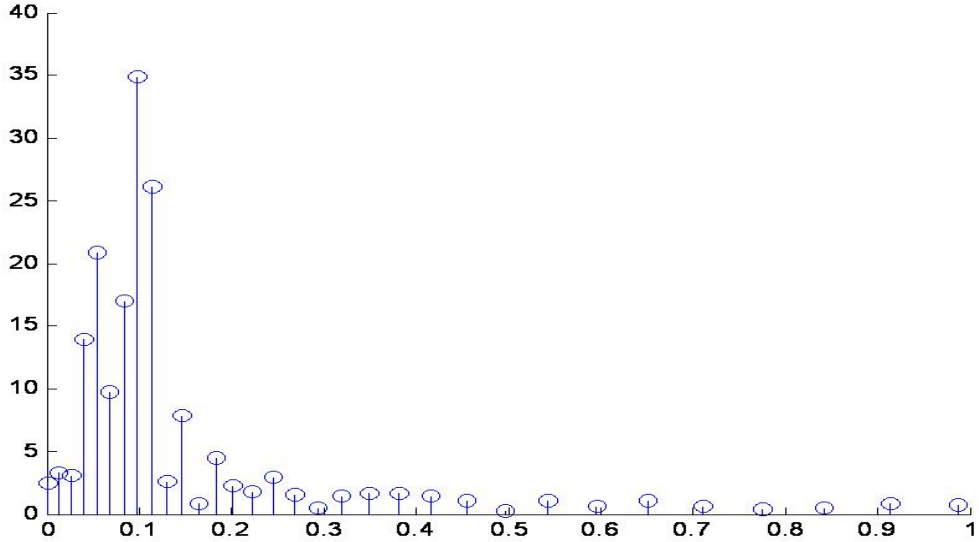

C

Figure 4-3. Continued

CHAPTER 5
FILTER BANKS USING ALLPASS TRANSFORMATION

5.1 Uniform DFT Filter Bank

Multirate systems often appear as a bank of filters where each filter maps the input into a baseband frequency subband [18]. The filter bank is a set of bandpass filters with either a common input or a summed output as shown in Figure 5-1. The structure of Figure 5-1 (A) is an *M*-band analysis filter bank with the subfilters $H_k(z)$ known as the analysis filters. It is used to decompose the input signal *x*[*n*] into a set of *M* subband signals $v_k[\mathrm{n}]$ with each subband signal occupying a portion of the original frequency band. On the other hand, a set of subband signals $\hat{v}_k[\mathrm{n}]$ occupying a portion of the original frequency band is combined into one signal *y*[*n*] as shown in Figure 5-1 (B), a synthesis filter bank, where each filter $F_k(z)$ is a synthesis filter.

An interesting application of this subband architecture is called a uniform DFT filter bank. The kth filter of a uniform DFT filter bank, denoted $H_k(z)$ in Figure 5-1 is defined in terms of H_0, called the prototype filter. Specifically

$$H_k(z) = H_0(W_M^k \cdot z),\ 0 \le k \le M-1. \tag{5.1}$$

The frequency response of the kth filter is given by

$$H_k(e^{j\omega}) = H_0(e^{j(\omega - 2\pi k/M)}),\ 0 \le k \le M-1. \tag{5.2}$$

It can be seen that the frequency response envelope of $H_0(z)$ filter is copied to new center frequencies located at $f_k = k \cdot f_s / M$, as shown in Figure 5-2. An interesting case occurs when $H_0(z)$ is defined as a multirate polyphase filter represented as:

$$H_0(z) = \sum_{m=0}^{M-1} z^{-m} P_m(z^M),\ 0 \le m \le M-1. \tag{5.3}$$

Equation (5.2) implies that:

$$H_k(z) = \sum_{m=0}^{M-1} W_M^{-im} z^{-m} P_m(z^M),\ \ 0 \le k \le M-1 \tag{5.4}$$

which has a DFT structure. That is:

$$h_k(n) = \sum_{j=0}^{M-1} W_M^{-ik} y_j[n] \tag{5.5}$$

where $y_j[n]$ is the output of the jth polyphase filter shown in Figure 5-3. Equivalently, it follows that $Y_m(z)=z^{-m}P_m(z^M)$. The polynomial outputs are combined using an *M*-point DFT, as shown in Figure 5-3(A), and are used to synthesize the frequency-selective filters $h_k(n)$. The DFT filter bank can, therefore, possess a number of known benefits including reduced arithmetic complexity when using a well designed DFT. To motivate this claim, consider that each filter $H_k(z)$ is on the order *N*. A filter bank would therefore require *MN* multiplies to complete a filter cycle. Each polyphase filter, however, is of order *N/M*, which reduces the complexity of each filter cycle to *MN/M*=*N* multiplies. That is, in *N* multiply cycles, all the intermediate values of $y_k(n)$ shown in Figure 5-3(A) can be computed. Adding decimators, as shown in Figure 5-3(B), the bandwidth requirement of each of the polyphase filters $H_k(z)$ can also be reduced. The multiply count of an *M*-point DFT would have to be added to this count to complete the multiply audit for a filter cycle. The multiply count of DFT is dependent of *M* and, for some choices, can be made extremely small. It can be noted that the data moving through the polyphase filters is slowed by a factor of *M* through decimation. By placing

decimators in the filter bank at the locations suggested in Figure 5-3(B), a further complexity reduction can be realized.

5.2 Non-uniform DFT Filter Bank

The non-uniform DFT filter bank can be built upon a uniform DFT filter bank infrastructure and an allpass filter transformation. The WDFT differentiates itself from the uniform DFT filter banks in that the signal to be transformed is pre-processed using the allpass filter *A(z)* prior to performing the DFT. The polyphase multirate filter architecture shown in Figure 5-4 was used by Galijasevic and Kliewer [19] to implement a non-uniform filter bank. For the case where $A(z)=1$, the design degenerates to a traditional uniform DFT filter bank [20, 21]. For the case where the polyphase filter terms are $P_i(z)=1$ (see Figure 5-4), the system is degenerated to an *M*-point DFT.

When the analysis subband filters are derived in terms of a prototype filter having an impulse response $h(n)$ and a set of allpass filters, a bank of complex modulated filter result. The transfer function of the kth subband filter $H_k(z)$ can be expressed as

$$H_k(z) = \sum_{m=0}^{M-1} W_M^{-im} A(z)^{-m} P_m(z^M), \quad 0 \le k \le M-1. \tag{5.6}$$

The resulting frequency response of a 16-channel system is motivated in Figure 5-5.

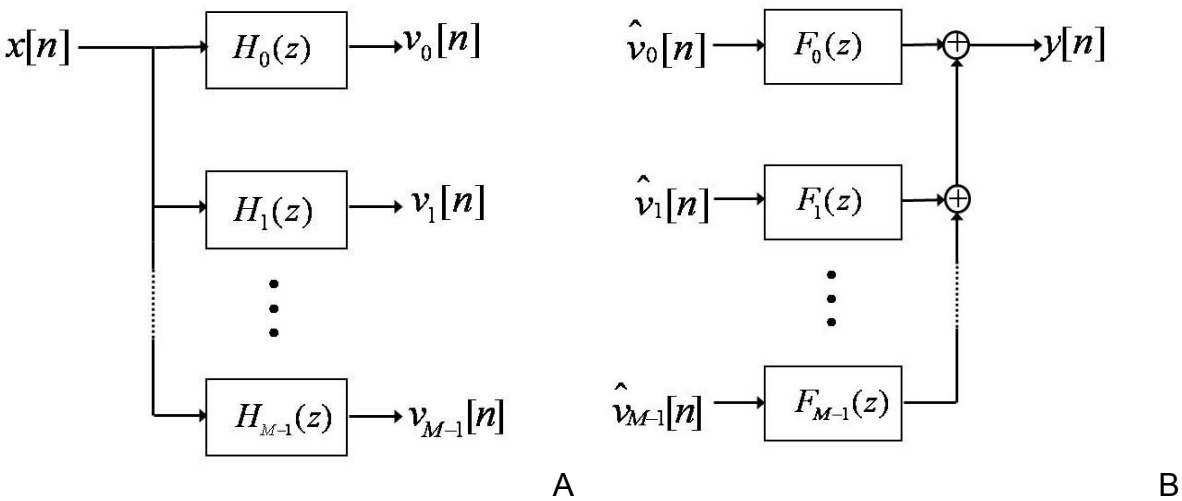

Figure 5-1. Typical subband decomposition system showing A) analysis filter bank, and B) synthesis filter bank.

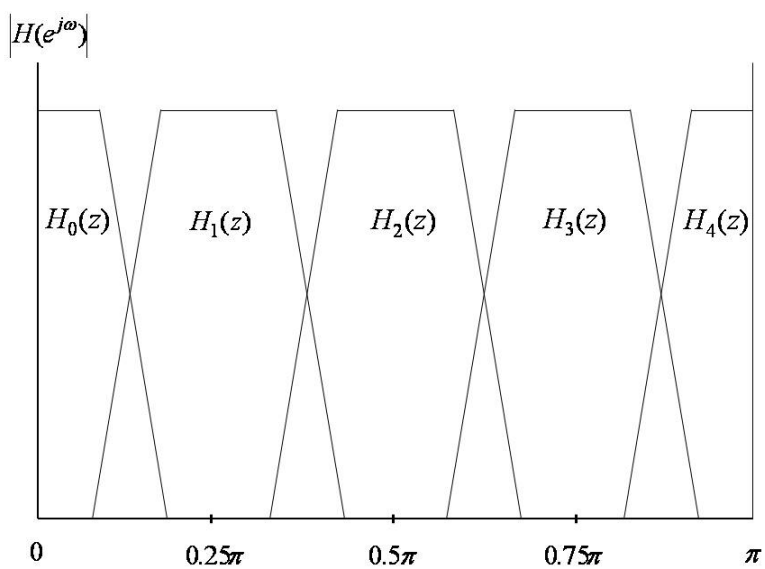

Figure 5-2. Uniform DFT filter bank magnitude frequency response for *M*=8.

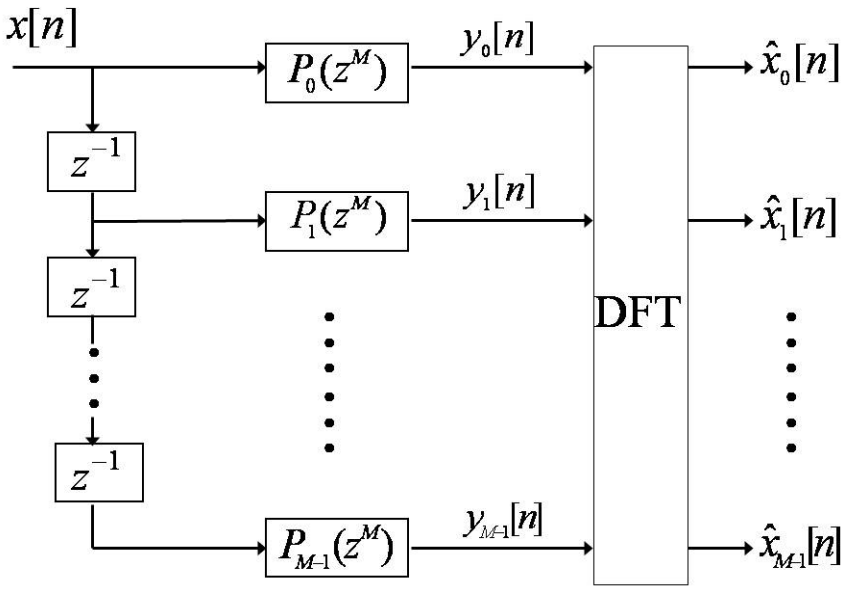

A

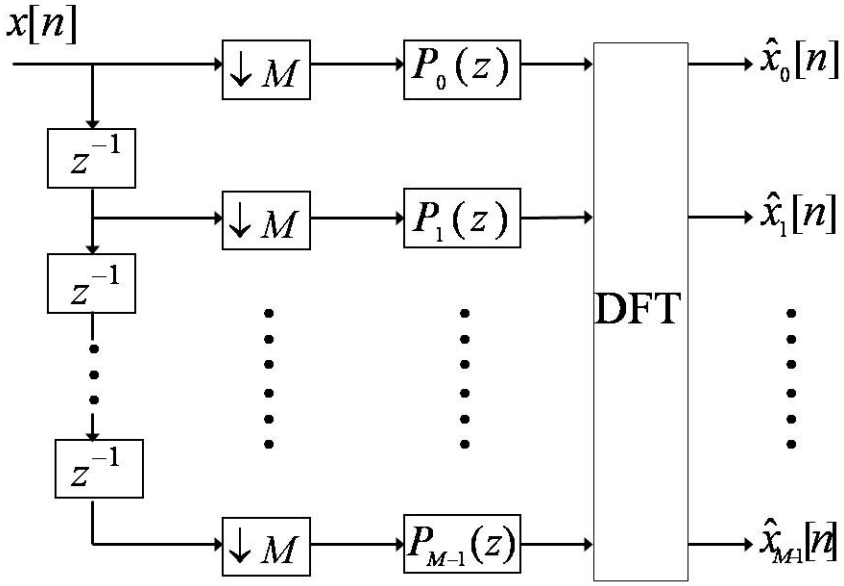

B

Figure 5-3. A) DFT filter bank and B) DFT filter bank with decimators

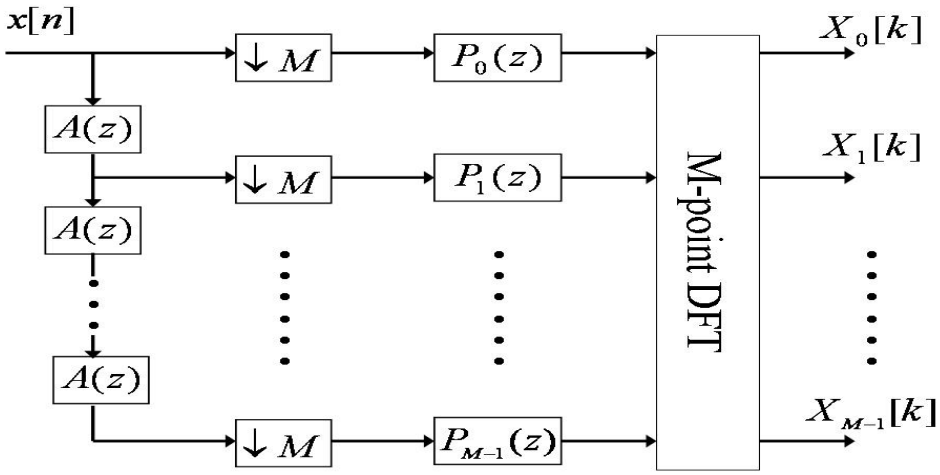

Figure 5-4. Non-uniform DFT filter bank

5.3 MATLAB Simulation

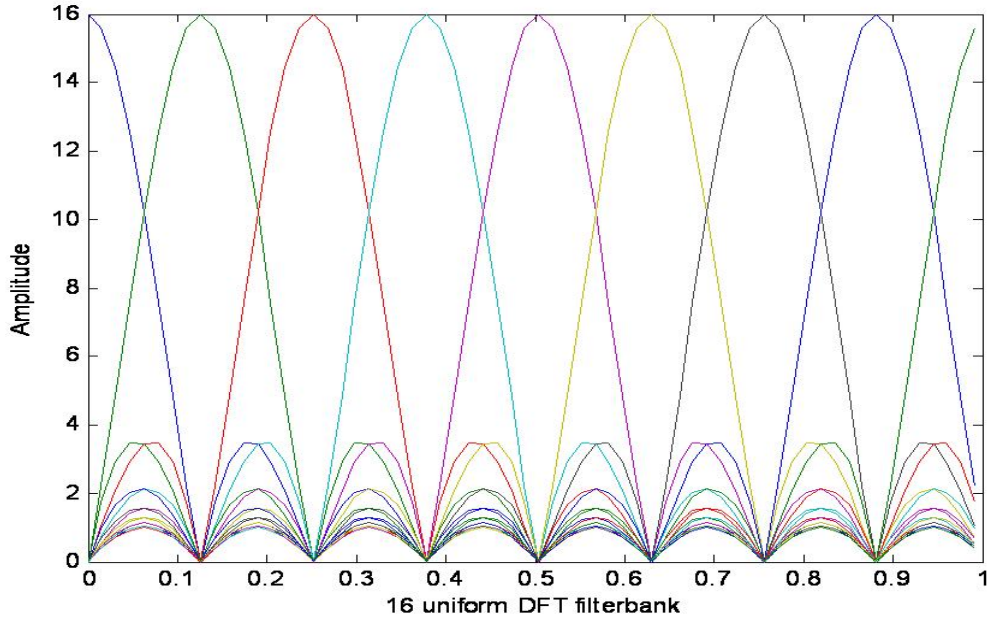

A

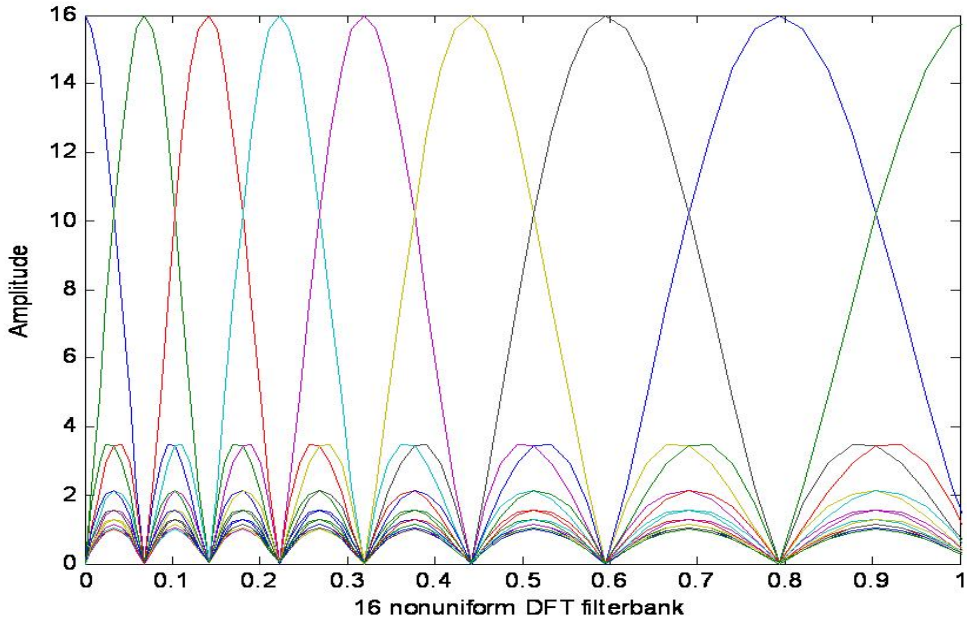

B

Figure 5-5. A) 16-channel uniform DFT filter bank, B) 16-channel non-uniform DFT filter bank for a=-0.3, and C) 16-channel non-uniform DFT filter bank for a=0.3.

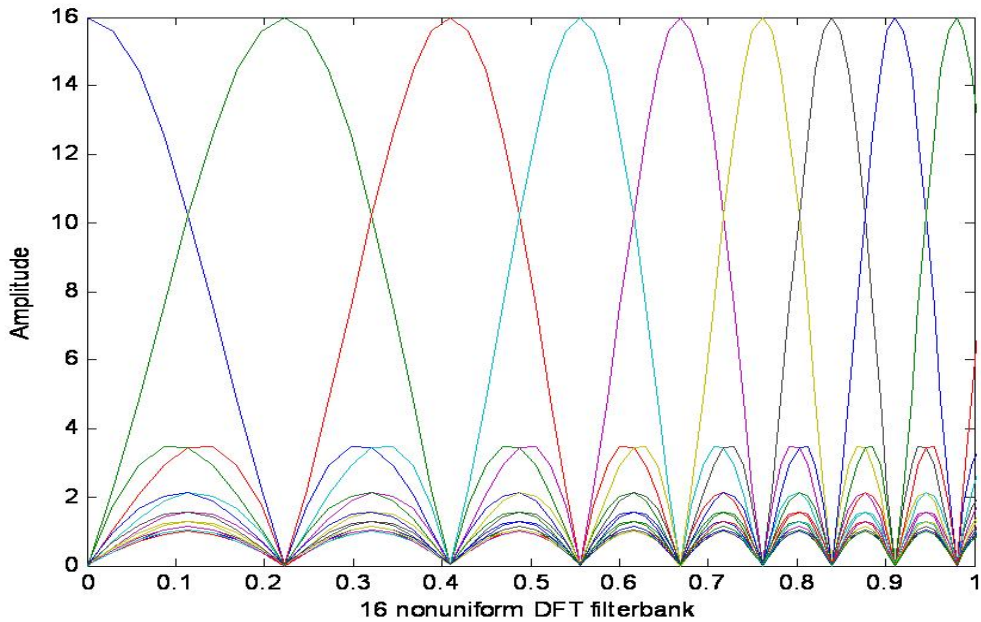

C

Figure 5-5. Continued

CHAPTER 6
PRELIMINARY STUDY AND RESULTS

6.1 FREQUENCY DISCRIMINATION

For spectral analysis applications, the DFT provides a uniform frequency resolution given by $\Delta = 2\pi / N$ over the normalized baseband $\omega \in [-\pi.\pi]$. The DFT's frequency resolution Δ is uniform across the baseband. This fact historically has limited the role of the DFT in performing acoustic and modal (vibration) signal analysis applications. These application areas prefer to interpret a signal spectrum in the context of logarithmic (octave) frequency dispersion. Another application area in which a fixed frequency resolution is a limiting factor is multi-tone signal detection and classification. It is generally assumed that if two tones are separated by 1.6Δ (1.6 harmonics) or less, then a uniformly windowed DFT/FFT cannot determine if one tone or multiple tones are present locally about a harmonic frequency. This problem is exacerbated when data widows are employed (*e.g.*, Hamming window). This condition is illustrated in Figure 6-1. In Figure 6-1(A), two tones separated by one harmonic (i.e., Δ) are transformed. The output spectrum is seen to consist of a single peak, losing the identification of each individual input tone because their main lobes get closer and eventually overlap. In the case reported by Figure 6-1(B), the two tones being transformed are separated in frequency by two harmonics (i.e., 2Δ). The presence of two distinct tones is now self-evident. In the case that two tones are not discriminated in Figure 6-1 (B), an increased resolution (increased *N*) is used to locally analyze the multi-tone signal. In fact, an increase in the DFT length improves the sampling accuracy by reducing the spectral separation of adjacent DFT samples, while it causes the higher computational complexity and cost penalty. In Figure 6-2 (A) and (B), it has been seen that the two

tones separated by 1.6 harmonics are unresolved with 64-point DFT, but resolved with 256-point DFT at the expense of increased complexity, respectively. So to resolve two tones without increasing the length of the DFT this dissertation proposes to exploit the WDFT as a frequency discrimination technology [22] that is operated using a control parameter a that locally defined frequency resolution as mentioned in Chapter 2. The effect of the warping relationship is demonstrated in Figure 6-3 which compares a DFT (a=0) to WDFTs for a=-0.071, a=-0.23 and a=-0.4 for the case where two tones are present separated by a single DFT harmonic. It is easily seen that by intelligently choosing the control parameter "a" the locally imposed frequency resolution can be expanded or contracted. To enhance the system's frequency discrimination, the frequency resolution should be maximized in the local region containing the input signals. As such, an intelligent agent will need to assign the best warping parameter "a" strategy, one that concentrates the highest frequency resolution in the spectral region occupied by the multi-tone process.

The next section describes the outcome of a preliminary study that compares two criteria and two search algorithms and develops an "intelligent" frequency resolution discrimination policy that can be used to improve multi-tone detection.

6.2 OPTIMIZATION OF FREQUENCY RESOLUTION

To optimize the choice the warping parameter "a", $|a|<1$, an intelligent search algorithm or agent is required. An initial search strategy is being evaluated and enabled using an optimal single-variable Fibonacci search and the modified Golden Section search techniques [23]. The search process is expected to iterate over a range of values of "a" that places a high local frequency resolution in the region occupied by multi-tone activity. To find the best warping parameter "a", two criteria of optimization

and cost functionals have been singled out for focused attention. The search methods iteratively restrict and shift the search range so as to optimize spectral resolution within a convergent range. The direction of the search is decided by the value of the cost functional at two points in the range. Two criteria studied to date are developed as follows.

A. Criterion #1

$$\Phi_1(\overline{\omega}) = \max\left[\overline{X}[k]\right] - \sum\left[\overline{X}[k]\Big|_{\overline{\omega}_b}\right] \tag{6.1}$$

where $\overline{\omega}_b$ is a frequency within the search interval and $\Phi_1(\overline{\omega})$ is designed to reward the local concentration of spectral energy and penalize more sparsely populated section of the spectrum. To obtain a locally optimal value of the warping parameter "a", the difference from the maximum value to average values between two adjacent spectral lines are computed using equation (6.1).

B. Criterion #2

$$\Phi_2(\overline{\omega}) = \sum\left[\sigma - \overline{X}[k]\right] \tag{6.2}$$

where σ is the threshold used to suppress leakage and $\Phi_2(\overline{\omega})$ is designed to reward the local concentration of spectral energy and minimize leakage determined by the relative amplitude of the main lobe and the side lobes to identify each individual input tone.

6.3 RESULTS AND COMPARISON

The dissertation reports on a multi-tone signal discrimination study conducted using two search methods, namely a Fibonacci search and a modified Golden Section search algorithm. Both are iterative methods that restrict and shift the searching range so as to determine an optimal operating point within a frequency range. Studies based

on these criteria involved presenting to the WDFT frequency discriminator two sinusoidal tones located at 0.157 and 0.314 rad/s. The search method was charged to find the “best” warping parameter. The comparison of results is shown in Table 6-1 and the evidence of this activity can be seen in Figure 6-5. To compare the temporal efficiency of each case, Table 6-1 also shows elapsed time needed to execute a search using MATLAB. The two tones, separated by one harmonic, were unresolved with 64-point DFT but resolved with 512-point DFT at the expense of increased complexity in Figure 6-4 (A) and (B), respectively. In Figure 6-5 (A)-(D), however, the two tones are shown to be present using 64-point WDFT. To calibrate the WDFT spectra, the locations of the actual two tones are also shown. Comparing the outcomes, a Fibonacci search was found to be the fastest and most effective in finding the “best” warping parameter using either search criteria. *Criterion #1* resulted in frequency resolution with a bigger variation according to search methods, while *Criterion #2* facilitated the optimization of the local resolution and identified the two tones closer to the actual locations of the tones.

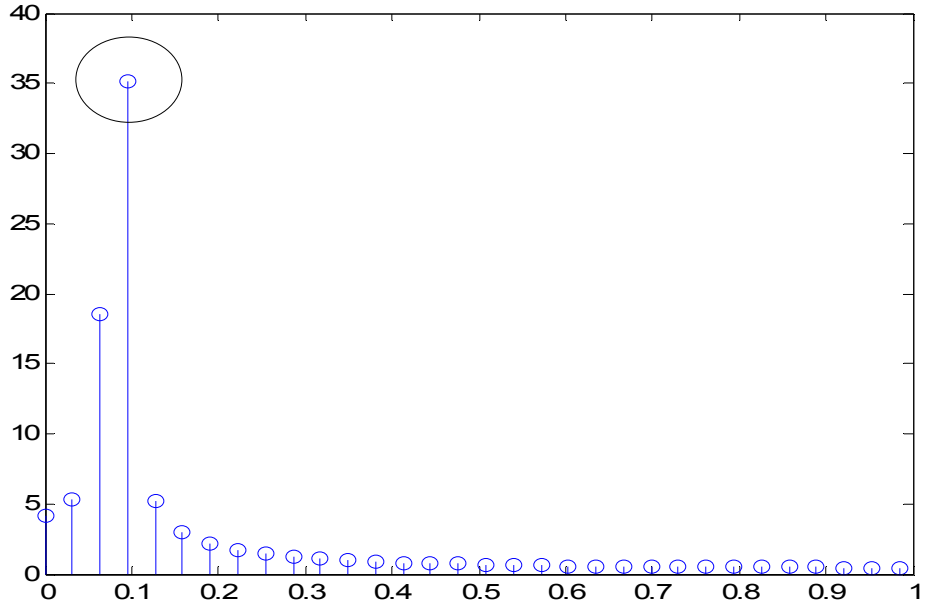

A

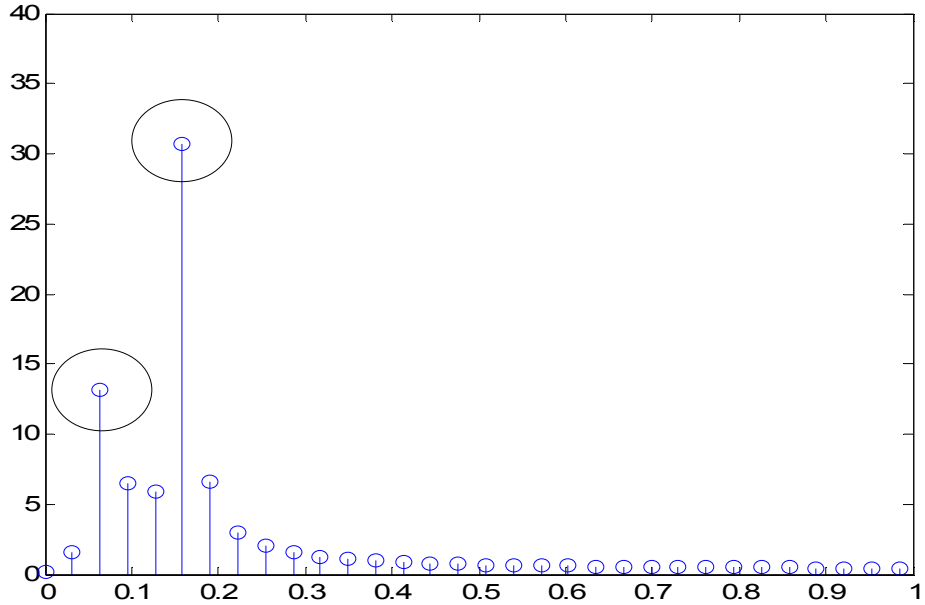

B

Figure 6-1. Magnitude spectrum for two tones separated A) by one harmonic and B) by two harmonics with 64-point DFT

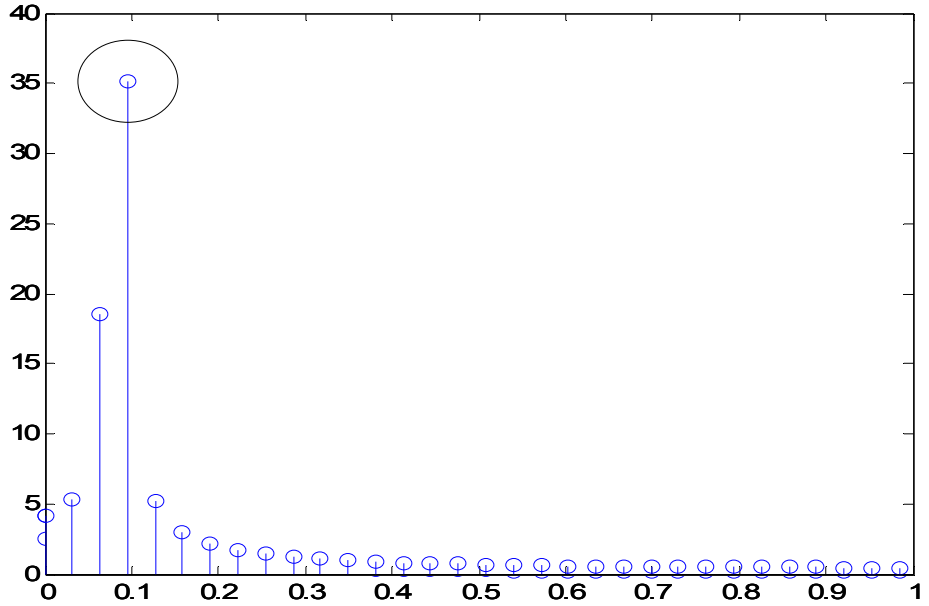

C

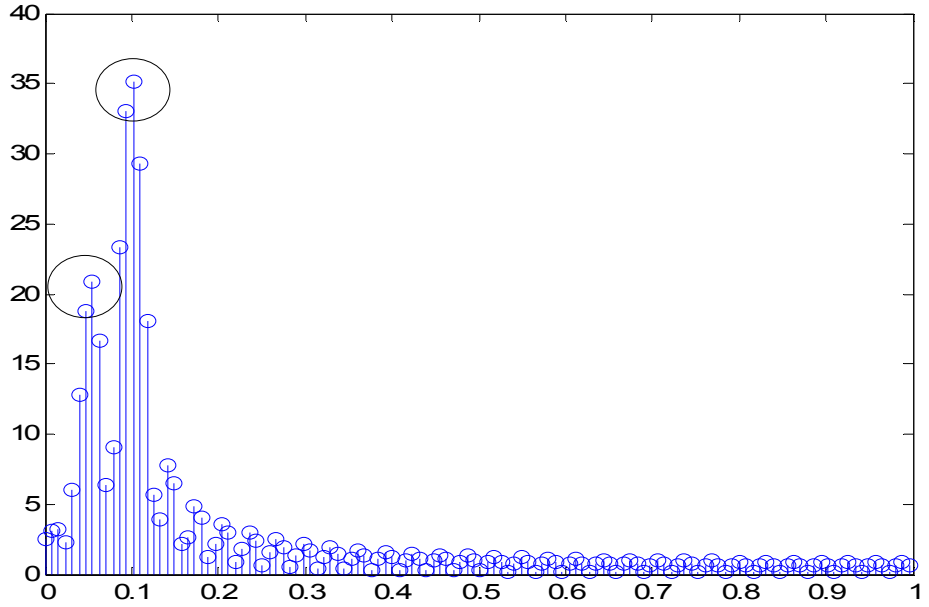

D

Figure 6-2. Magnitude spectrum for two tones separated by 1.6 harmonics A) with 64-point DFT and B) with 256-point DFT

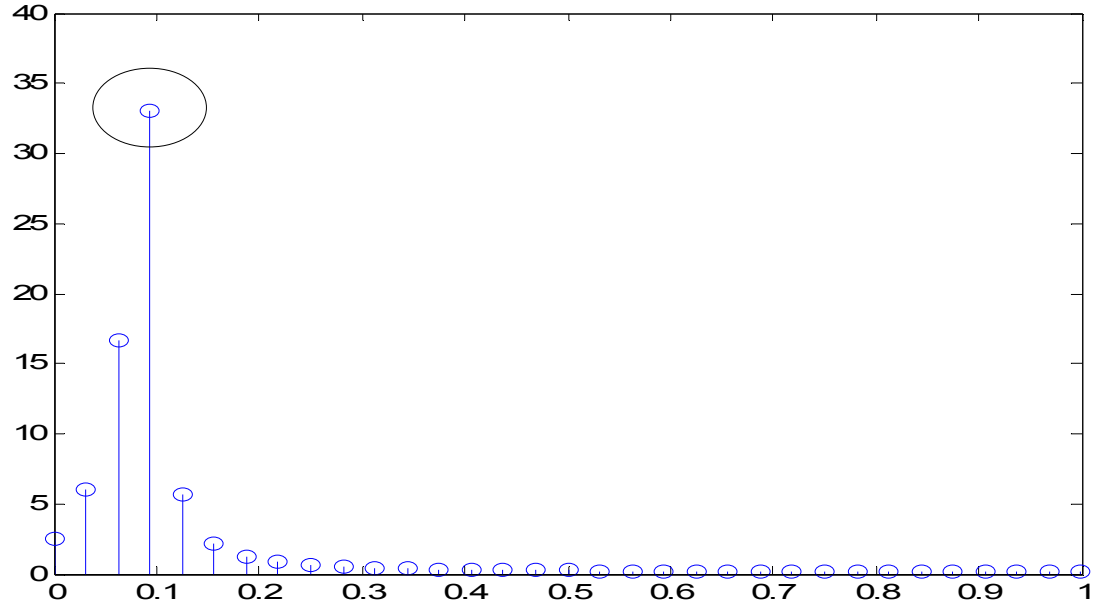

A

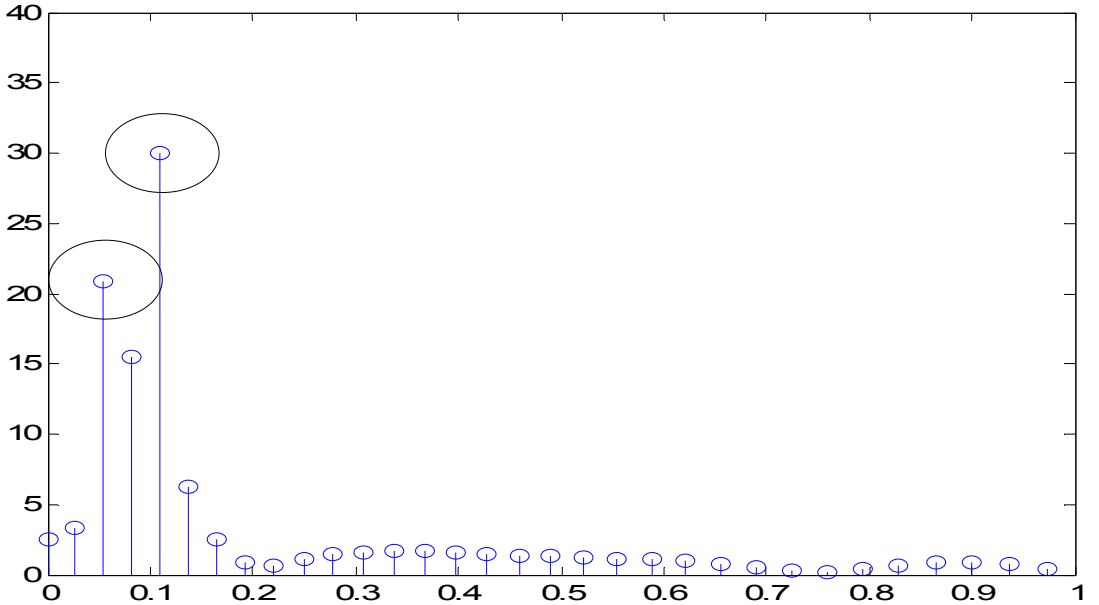

B

Figure 6-3. Magnitude spectrum for two tones with 64-point WDFT with (A) a = 0, (B) a = -0.071, (C) a = -0.23, and (D) a = -0.40.

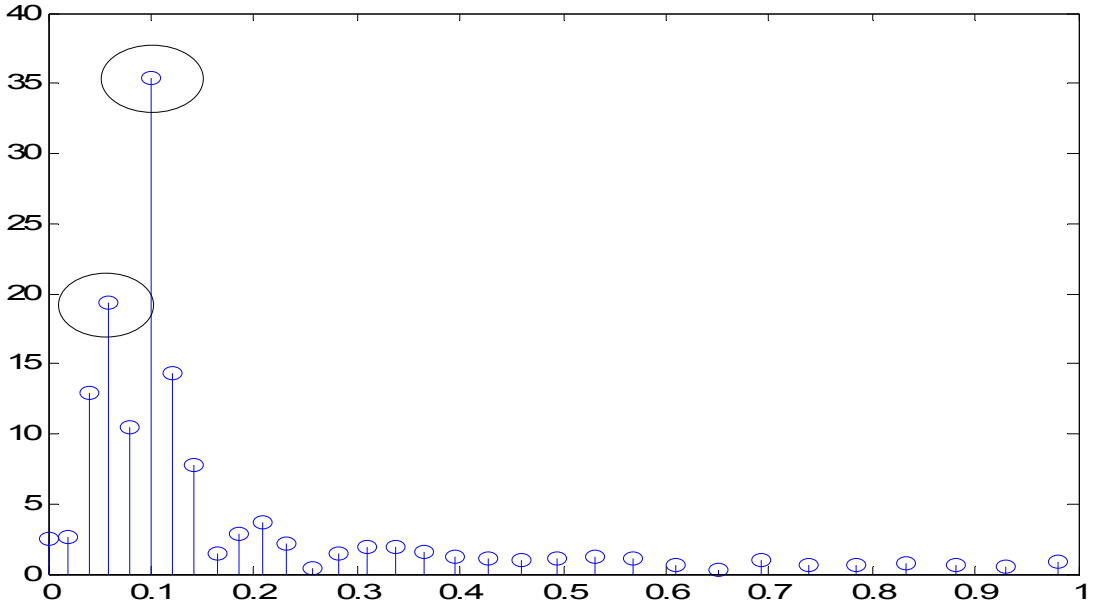

C

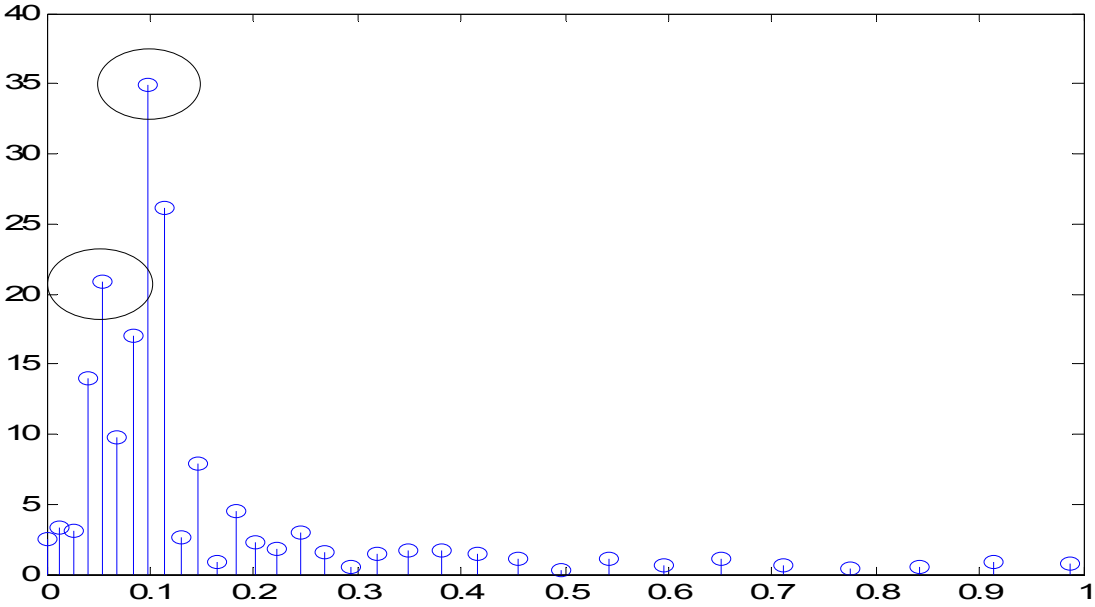

D

Figure 6-3. Continued

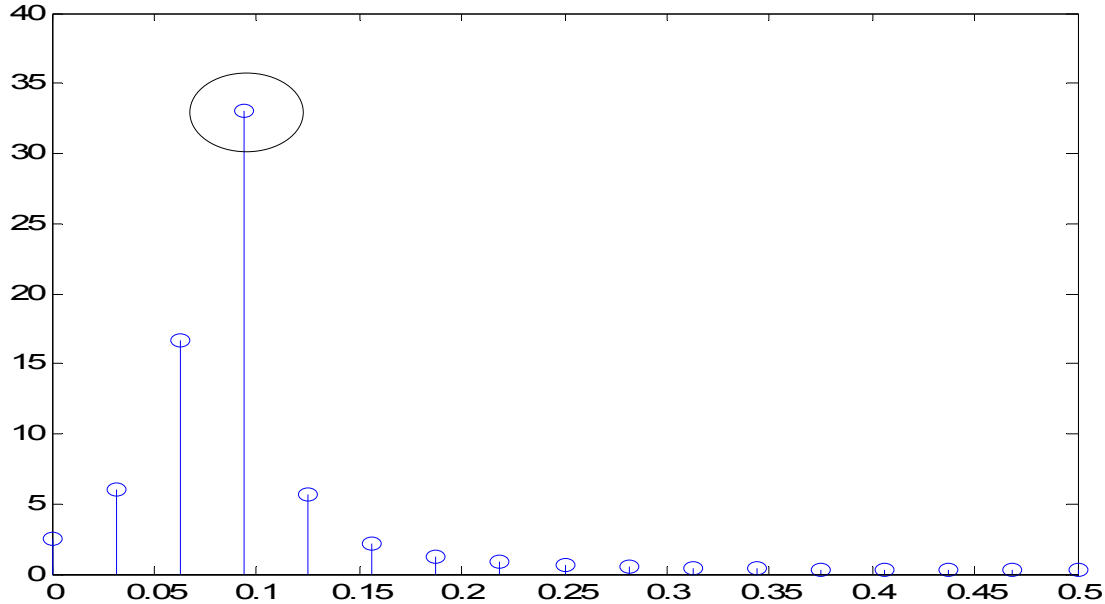

A

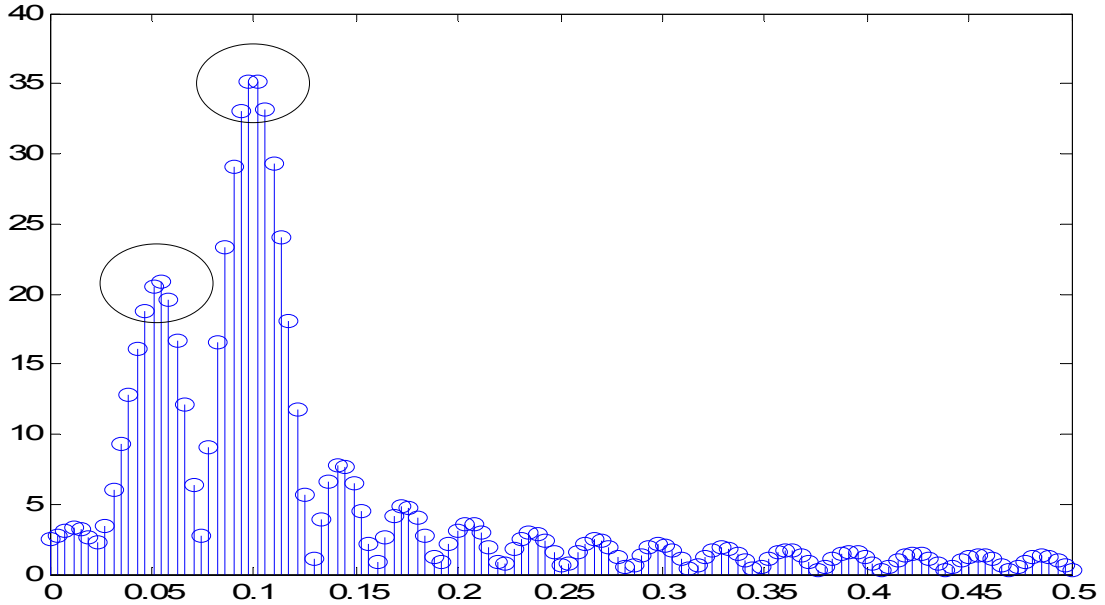

B

Figure 6-4. Magnitude spectrum for two tones separated by 1.6 harmonics A) with 64-point DFT (a=0) and B) with 512-point DFT (a=0).

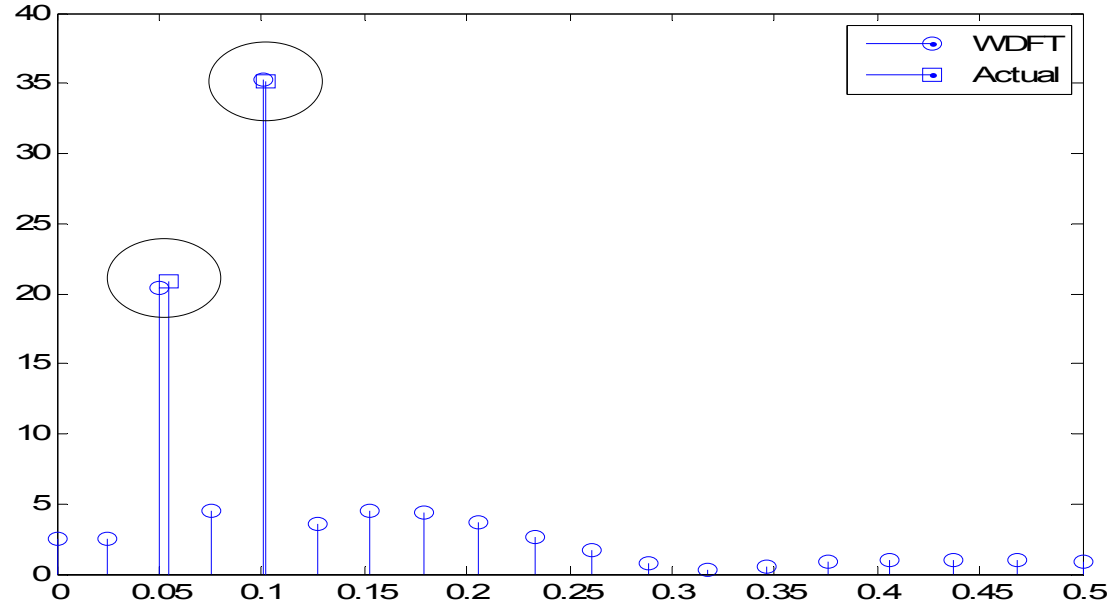

A

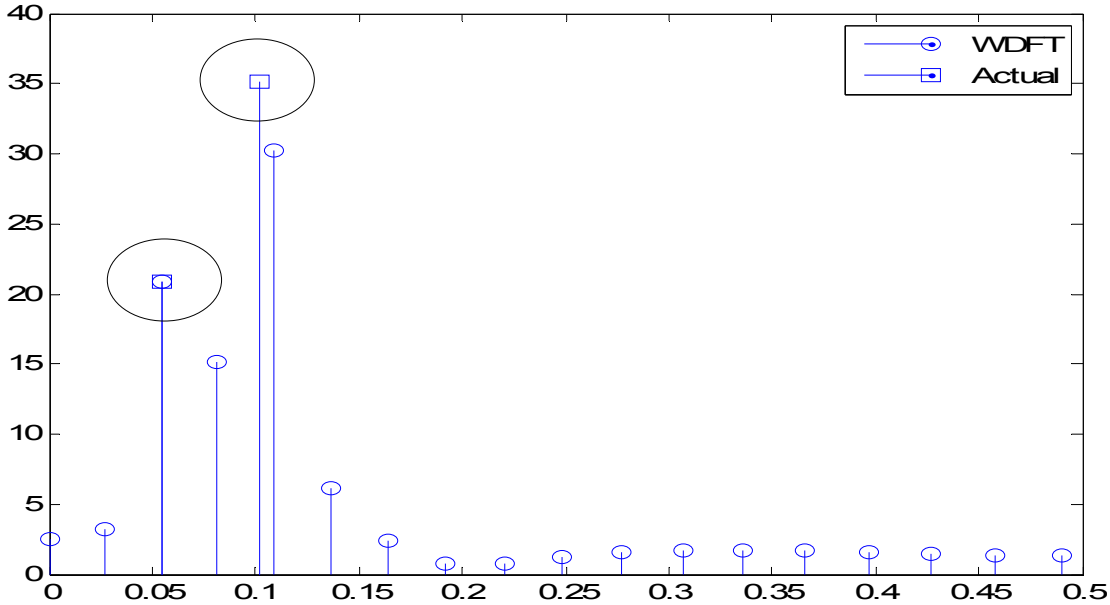

B

Figure 6-5. Magnitude spectrum for two tone detection with 64-point WDFT with A) a=-0.1087 , B) a=-0.0721, C) a=-0.0996, and D) a=-0.1381.

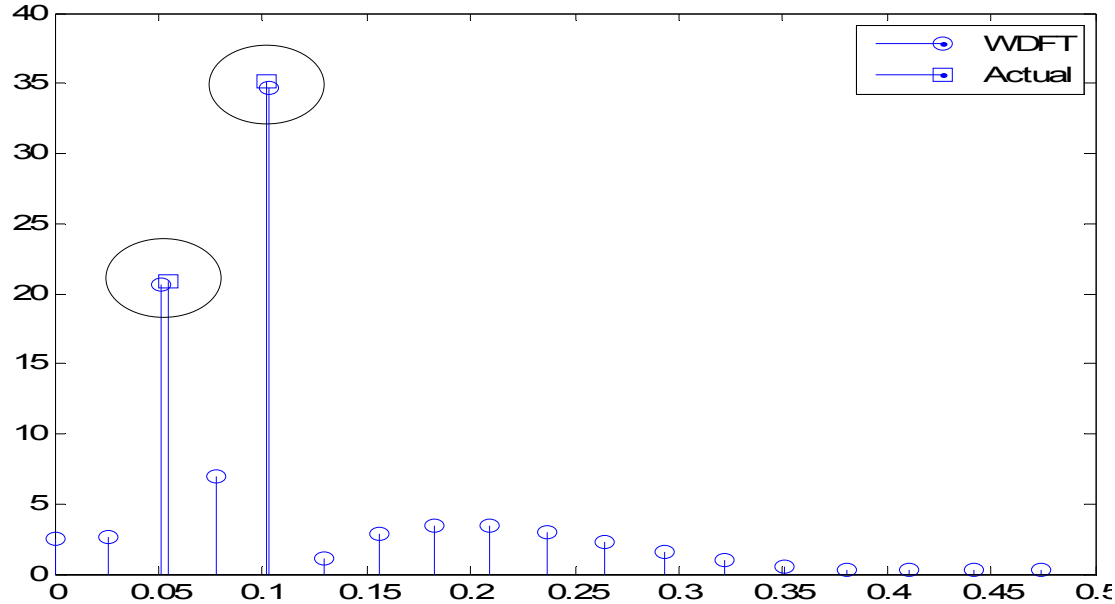

C

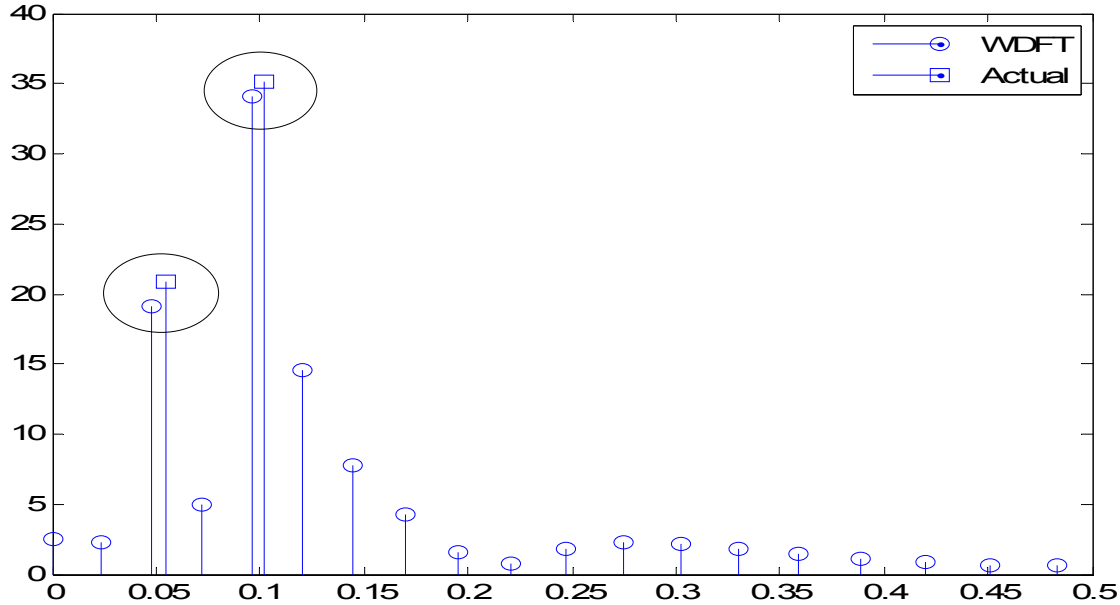

D

Figure 6-5. Continued

Table 6-1. Comparison of the warping parameter

Criterion	*Criterion #1*		*Criterion # 2*	
Search Method	Fibonacci search	M. Golden section search	Fibonacci search	M. Golden section search
Warping parameter	a = -0.1087	a = -0.0721	a = -0.0996	a = -0.1381
Elapsed time (sec.)	t = 0.749252s	t = 0.888743s	t = 0.736151s	t = 0.751035s

CHAPTER 7
CONCLUSIONS AND FUTURE WORK

7.1 Conclusions

This dissertation aims at exploring spectral analysis using the warped discrete Fourier transform (WDFT) compared to a conventional discrete Fourier transform (DFT). It focuses on detecting multiple narrowband signals which are not able to be isolated with uniform frequency resolution and optimizing the local frequency resolution by finding the best warping control strategy. And the system developed and tested also focuses on maximizing the WDFT frequency resolution over those frequencies that exhibit a localized concentration of spectral energy and, implicitly, diminishing the importance of other frequency ranges. This dissertation demonstrates that multi-tone signals are able to be more readily detected and discriminated by externally controlling the frequency resolution of the WDFT in intelligent manners using optimal single-variable search techniques, a Fibonacci search and a modified Golden Section search.

Finally, this dissertation shows the best frequency resolution reducing spectral leakage which obscures the spectral separation between of adjacent DFT harmonics due to the finite frequency resolution of the DFT without increasing the DFT length for multi-tone detection using the WDFT. In fact, an increase in the DFT length improves the sampling accuracy by reducing the spectral separation of adjacent DFT samples, while it brings up the higher computational complexity and cost penalty. In order to minimize and suppress spectral leakage the WDFT is exploited to control the spectral separation through the warping parameter.

Moreover, the usage of the WDFT presents obtaining higher and optimized local frequency resolution through finding the best warping control strategy. In general, a

uniformly windowed DFT/FFT cannot determine if one tone or multiple tones are present locally about a harmonic frequency for two tones separated by 1.6 Δ (1.6 harmonics) or less. It shows that, however, the WDFT can discriminate between two signals separated by as little as 1.3 harmonics.

Overall, the new spectral analysis technology using the WDFT results in a higher local resolution, less computational complexity, more capability, and lower cost.

7.2 Future work

Based on the frequency discrimination for multi-tone signal detection using the WDFT, the proposed spectral analyzer design holds the promise of lower complexity. This can be translated into low power and/or high speed. Future work should focus on quantifying this advantage in a physical instantiation. The design outcome can then be benchmarked against a commercial unit and performance advantages directly measured.

Another area that may prove productive is developing auto-configuration software or MATLAB attachments that will optimize a design outcome based on a set of specifications.

LIST OF REFERENCES

[1] A. V. Oppenheim and R. W. Schafer, Discrete-Time Signal Processing. Englewood Cliffs, NJ, Prentice-Hall, 1989.

[2] B. Evans, Dual Tone Mulitple Frequencies, U.C. Berkeley, http://ptolemy.eecs.berkeley.edu/papers/96/dtmf_ict/www/nodel.html

[3] G. Goertzel, An algorithm for evaluation of finite trigonometric series. American Mathematical Monthly, vol. 65, Jan. 1958, pp. 34-35.

[4] E. A. Hoyer, R. F. Stork, The zoom FFT using complex modulation, *Proceedings IEEE ICASSP*, vol. 2, 1977, pp. 78-81.

[5] Y. Tadokoro, K. Abe, Notch Fourier transform, *IEEE transactions Acoustics Speech Signal Processing*, vol. ASSP-35, no. 9, Sep. 1987, pp.1282-1288.

[6] C. Braccini, A. Oppenheim, Unequal Bandwidth Spectral Analysis using Digital Frequency Warping, *IEEE transactions Acoustics Speech Signal Processing*, vol. ASSP-22, no. 4, Aug. 1974, pp. 236-244.

[7] A. Makur, S. K. Mitra, Warped discrete-Fourier transform: Theory and applications. *IEEE Transactions on Circuits Systems, vol. 48*, Sep. 2001, pp. 1086-1093.

[8] R. Kumaresan. Spectral analysis. In S.K. Mitra and J.F. Kaiser, editors, Handbook for Digital Signal Processing, chapter 16, pp. 1143-1242, Wiley-Interscience, New York NY, 1993.

[9] J. G. Proakis, D. G. Manolakis, Digital Signal Processing: Principles, Algorithms and Applications, 3rd ed. New Jersey: Prentice Hall, 1995.

[10] S. K. Mitra, Digital Signal Processing: A Computer-Based Approach, 2nd ed. New York: McGraw-Hill, 2001.

[11] F. J. Harris, On the Use of Windows for Harmonic Analysis with the Discrete Fourier Transform, Proceedings of the IEEE, vol. 66, pp. 51-83, January 1978.

[12] T. Saramäki, Finite impulse response filter design, In S. K. Mitra and J. F. Kaiser, editors, Handbook for Digital Signal Processing, chapter 4, pp. 155-277, Wiley-Interscience, New York NY, 1993.

[13] A. Oppenheim and D. Johnson, Computational of spectra with unequal resolution using the fast Fourier transform, *Proc*, *IEEE*, vol. 59, pp. 209-301.

[14] S. Baghci and S. K. Mitra, Nonuniform Discrete Fourier Transform and its signal processing Applications. Norwell, MA: Kluwer, 1999.

[15] G. H. Golub, C. F. Van Loan, Matrix Computations, third edition, Johns Hopkins University Press, 1996

[16] S. Franz, S. K. Mitra, J. C. Schmidt, G. Doblinger, Warped discrete Fourier transform: a new concept in digital signal processing, *Proceedings IEEE ICASSP*, vol. 2, pp.1205-1208, 2002

[17] A.C. Constantinides, Spectral transformations for digital filters, *Pro. Inst. Elect. Eng., vol. 117, no.8*, 1970 pp. 1585-1590

[18] P. P. Vaidyanathan, Multirate Systems and Filter Banks, Englewood Cliffs, NJ: Prentice Hall, 1993.

[19] E. Galijasevic, and J. Kiel, Design of Allpass-Based Non-Uniform Oversampled DFT Filter Banks, IEEE ICASSP, Orlando, FL, May 2002, pp 1181-1184.

[20] F. Taylor and J. Mellott, Hands-On Digital Signal Processing, McGraw Hill, 1998.

[21] A. Williams and F. Taylor, Electronic Filter Design Handbook, 4th Ed., McGraw Hill, 2006.

[22] Ohbong Kwon, Fred Taylor, Multi-tone Detection Using the Warped Discrete Fourier Transform, MWSCAS, Knoxville, TN, Aug. 2008

[23] Ralph W. Pike, Optimization for Engineering Systems, Van Nostrand Reinhold company, 2001, http://www.mpri.lsu.edu/bookindex.html

BIOGRAPHICAL SKETCH

Ohbong Kwon was born in Guelph, Canada and has grown up in Seoul, South Korea. He received both his B.S. degree and M.S. degree in electrical engineering from Hanyang University, South Korea in 1998 and 2000, respectively.

He was in the High Speed Digital Architecture Laboratory (HSDAL) in the Electrical and Computer Engineering Department at the University of Florida during his PhD study. His present research interests are in the areas of signal processing, digital filter design, and optimization.